UNIVERSITY OF WEST BOHEMIA

FACULTY OF APPLIED SCIENCES

DEPARTMENT OF MECHANICS

DIPLOMA THESIS

INFLUENCE OF ANISOTROPY DETERMINATION ON SHEET METAL FORMING SIMULATIONS

Adam Hybler

May 31, 2025

Declaration

I declare that I prepared the diploma thesis independently and that I have indicated the literature used and all the sources from which I drew.

In Pilsen 31. 5. 2025 Adam Hybler

Acknowledgement

I would like to express my gratitude to COMTES FHT a.s. for providing the facilities, materials, and invaluable support, ranging from experimental measurements and samples to expert consultations, that were essential to the successful completion of this thesis. I also wish to extend my sincere appreciation to my supervisor, Ing. Martin Zajíček, Ph.D., for his insightful guidance, constructive feedback, and excellent collaboration throughout the course of this work.

ZÁPADOČESKÁ UNIVERZITA V PLZNI
Fakulta aplikovaných věd
Akademický rok: 2024/2025

ZADÁNÍ DIPLOMOVÉ PRÁCE

(projektu, uměleckého díla, uměleckého výkonu)

Jméno a příjmení:	**Bc. Adam HYBLER**
Osobní číslo:	**A22N0023P**
Studijní program:	**N0715A270006 Aplikovaná mechanika**
Specializace:	**Dynamika konstrukcí a mechatronika**
Téma práce:	**Vliv určení anizotropie materiálu na simulace tváření plechů**
Zadávající katedra:	**Katedra mechaniky**

Zásady pro vypracování

1. Přehled současného stavu problematiky.
2. Experimentální vyhodnocení anizotropie plechů pro materiál DP1000.
3. Numerické simulace testu hlubokého tažení s využitím kritérií plasticity Hill48 a Yld2004-18p.
4. Porovnání výsledků numerických simulací a experimentů.

Rozsah diplomové práce: **40 – 60 stran A4**
Rozsah grafických prací:
Forma zpracování diplomové práce: **tištěná**
Jazyk zpracování: **Angličtina**

Seznam doporučené literatury:

1. Banabic, D.: Sheet metal forming processes – Constitutive modelling and numerical simulation, Springer-Verlag, Berlin, 2010.
2. Habraken, A.M.: Analysis of ESAFORM 2021 cup drawing benchmark of an Al alloy, critical factors for accuracy and efciency of FE simulations, International Journal of Material Forming 15 (5) (2022), 61.
3. Wang, Ch., Li, D., Meng, B., Wan, M.: Effect of anisotropic yield functions on prediction of critical process window and deformation behavior for hydrodynamic deep drawing of aluminum alloys, Metals 10 (4) (2020), 492.
4. Marciniak, Z.: Mechanics of sheet metal forming (Second edition), Butterworth-Heinemann, 2002.
5. Hill, R.: A theory of yielding and plastic flow of anisotropic metals, Proceedings of the Royal Society of London A193 (1948), 281-297.

Vedoucí diplomové práce: **Ing. Martin Zajíček, Ph.D.**
Katedra mechaniky

Datum zadání diplomové práce: **14. října 2024**
Termín odevzdání diplomové práce: **31. května 2025**

Západočeská univerzita v Plzni
L.S.
Fakulta aplikovaných věd

Doc. Ing. Miloš Železný, Ph.D.
děkan

Prof. Ing. Jan Vimmr, Ph.D.
vedoucí katedry

V Plzni dne 14. října 2024

Abstract

This thesis investigates the influence of anisotropy models and yield point identification methods on the accuracy of sheet metal forming simulations, specifically for the high-strength steel DP1000. Two anisotropic yield criteria, Hill48 and Yld2004-18p, are compared under the conditions of a deep drawing circular cup test. Multiple yield point determination approaches are evaluated, among them standard mechanical methods and temperature based techniques. Finite element analyses using calibrated material models are carried out and validated through experiments, and their predictive accuracy is assessed based on earing profiles. The results indicate that while more advanced anisotropic model Yld2004-18p offers wider options for adapting to the real behavior of the material, its performance is highly dependent on the quality of the input experimental data. On the other hand, simpler model Hill48 demonstrates comparable or even superior performance under the conditions present. The findings highlight the importance of minimizing relative variations in yield strength and Lankford coefficient across different material orientations rather than focusing on absolute values when developing or selecting material models for forming simulations.

Abstrakt

Tato diplomová práce zkoumá vliv modelů anizotropie a metod určování meze kluzu na přesnost simulací tváření plechů, konkrétně pro vysokopevnostní ocel DP1000. Celkem jsou porovnávána dvě anizotropní kritéria plasticity, Hill48 a Yld2004-18p, a to konkrétně za podmínek hlubokého tažení při kalíškové zkoušce. Hodnoceno je několik přístupů určení meze kluzu, mezi nimi standardní mechanické metody a metody založené na měření teploty. Za pomoci metody konečných prvků jsou provedeny analýzy, včetně experimentálního ověření, které využívají kalibrované materiálové modely. Přesnost analýz je hodnocena na základě profilu zvlnění okraje kruhového výtažku. Výsledky ukazují, že přestože pokročilejší anizotropní model Yld2004-18p nabízí širší možnosti přizpůsobení reálnému chování materiálu, jeho spolehlivost výrazně závisí na kvalitě vstupních experimentálních dat. Naproti tomu jednodušší model Hill48 vykazuje za daných podmínek srovnatelnou, nebo dokonce lepší shodu s experimenty. Na základě dosažených poznatků z této práce lze učinit závěr o významu minimalizace relativních rozdílů v mezích kluzu a Lankfordových koeficientech v různých materiálových směrech. Při vývoji či výběru materiálových modelů pro simulace tváření se zdá být vhodnější soustředit se na tyto rozdíly než na absolutní hodnoty těchto parametrů.

Contents

List of used symbols and abbreviations

Symbol used	SI Unit	Name
YP	[-]	Yield point
RD	[-]	Rolling direction
TD	[-]	Transverse direction
$\boldsymbol{\varepsilon}$	[-]	Tensor of total true strain
$\boldsymbol{\varepsilon_e}$	[-]	Elastic component of total true strain
$\boldsymbol{\varepsilon_p}$	[-]	Plastic component of total true strain
$\boldsymbol{\sigma}$	[Pa]	Cauchy's stress tensor
σ_{ij}	[Pa]	Components of Cauchy's stress tensor
$\boldsymbol{E}$	[Pa]	Tensor of elastic constants
σ	[Pa]	True stress
ε	[-]	True strain
ε_p	[-]	True plastic strain
E	[Pa]	Young's modulus
T	[K]	Current temperature
ΔT	[K]	Temperature change
c_p	[J kg^{-1} K^{-1}]	Specific heat capacity at constant stress
f	[-]	Plastic anisotropy function
α	[K^{-1}]	Coefficient of linear thermal expansion
$\Delta\sigma$	[Pa]	Stress change
ρ	[kg m^{-3}]	Density
h_{ij}	[-]	Constants for anisotropic von Mises model
F, G, H, L, M, N	[-]	Constants coefficients for anisotropic models
X, Y, Z	[Pa]	Tensile yield strengths in principal directions
T	[Pa]	Shear yield strength
σ_i	[Pa]	Principal stresses
σ_0	[Pa]	Reference tensile yield strength
τ_0	[Pa]	Reference shear yield strength
R_{ij}	[-]	Anisotropic yield strength ratios used in Abaqus
$d\lambda$	[-]	Hardening parameter
θ	[°]	Angle from RD
r_θ	[-]	Lankford coefficient of tensile specimen under angle θ
$\tilde{\sigma}_\theta$	[Pa]	Yield strength of tensile specimen under angle θ
ε_w^p	[-]	True plastic strain across specimen width
ε_t^p	[-]	True plastic strain across specimen thickness
σ_θ	[Pa]	Stress in tensile specimen under angle θ
w_i	[-]	Weight coefficients for error function
$\boldsymbol{S}$	[Pa]	Deviatoric stress tensor
$\boldsymbol{\tilde{S}'}$	[Pa]	First linear transformation of deviatoric stress tensor

Symbol used	SI Unit	Name
$\tilde{S}_i'$	[Pa]	Principal value of first linear transformation of deviatoric stress tensor
$\boldsymbol{\tilde{S}''}$	[Pa]	Second linear transformation of deviatoric stress tensor
$\tilde{S}_i''$	[Pa]	Principal value of second linear transformation of deviatoric stress tensor
$\hat{\boldsymbol{\sigma}}$	[Pa]	Stress vector
$\hat{\boldsymbol{S}}$	[Pa]	Deviatoric stress vector
$\boldsymbol{T}$	[-]	Transformational matrix
$\boldsymbol{C'}$	[-]	First linear transformational matrix
$\boldsymbol{C''}$	[-]	Second linear transformational matrix
m	[-]	Exponent dependent on material structure
c_{ij}'	[-]	Coefficients of first linear transformation
c_{ij}''	[-]	Coefficients of second linear transformation
d_1, d_2, d_s	[m]	Diameters of deep drawing cup test
R_1, R_2	[m]	Radii of deep drawing cup test
t	[m]	Thickness of the sheet
w, k	[m]	Dimensions of the die relief in deep drawing cup test
ψ	[°]	Angle of relief in deep drawing cup test
DIC	[-]	Digital image correlation
a, b, c	[-]	Parameters of sinus model for description of cup tilt
ALLAE	[J]	Total energy dissipated as artificial strain energy in Abaqus
ALLSE	[J]	Total stored elastic energy in Abaqus
ALLKE	[J]	Total kinetic energy in Abaqus

1 Introduction

In the quest for lighter, stronger, and more sustainable materials, the precision and control of metal forming processes have become more critical than ever. Numerical simulation of these processes is essential to minimize lead time, as emphasized in [1]. Phenomena such as springback and anisotropy naturally arise during material formation and require particular attention when working with high-strength materials, making accurate simulations irreplaceable, as highlighted in [2].

To effectively simulate forming processes, advanced software simulation tools rely on highly accurate material models. A key factor in these models is the anisotropy of the material, often described by the yield surface. Although the yield surface provides a framework for understanding material behavior, standard isotropic models often fail to capture the complexities of anisotropic materials. Characterizing the yield surface requires experimental data from various tests, with the uniaxial tensile test being the most common method [3, 4]. In this test, the yield point (YP) of a material is measured in specific directions relative to its rolling direction, providing essential data for calibrating analytical models that simulate material behavior in forming processes.

During the forming process of modern materials, such as high-strength steels and advanced aluminum alloys, springback is a significant phenomenon that is notoriously difficult to predict. To address the challenge of accurately predicting springback, some studies suggest using complex models of material behavior. The biggest challenge is the correct determination of nonlinear elastic strain region and potentially other intermediate states of material behavior between elasticity and plasticity. For example in [5], the concept of Quasi-Plastic-Elastic strain is introduced as an intermediate state between elasticity and plasticity, which was later extended for multi-axial stress scenarios as the Quasi-Plastic--Elastic surface in [6]. This study uses the idea of a homogeneous anisotropic hardening model that predicts kinematic hardening using isotropic hardening laws from [7]. This model behaves the same as isotropic hardening law when monotonic deformation occurs. However, most of the current software tools still use the standard elasto-plastic model and that is why the determination of YP is still very important to springback prediction and accurate anisotropic models.

Multiple attempts have been made to capture the transition from the linear elastic region to the nonlinear elasto-plastic region. Most methods rely on the strain-stress curve obtained from uniaxial tensile tests for this identification. The standard ISO 6892-1, for instance, defines this transition using a percentage (50%) of the offset yield strength corresponding to 0.2% plastic strain. This approach is of course iterative. Another method using the strain-stress curve is the method developed by Merklein in [8], where the area below the curve is calculated by two different approaches, detecting the beginning of nonlinear behavior. Some of the newer approaches aim to identify the onset of yielding by measuring the temperature of the specimen. During elastic deformation, the temperature decreases, whereas in the plastic region, it increases [9, 10, 11, 12].

While YP is important for identifying the transition from the elastic to the elasto-plastic region, this transition is often influenced by the angular orientation within the sheet metal's plane. A phenomenon referred to as planar anisotropy [1]. For sheet metals, the thickness direction is typically negligible, reducing the yield surface to a curve in the $\widehat{\sigma_{11}\sigma_{22}}$ plane. For isotropic materials, various criteria, such as the von Mises or Tresca criterion, can be

applied. However, these options are limited because most materials do not exhibit purely isotropic behavior.

One of the most simple models for the description of anisotropy is Hill48. This model only uses parameters from 3 directions and has 3 orthogonal planes of symmetry and therefore is suitable for orthotropic materials. It was introduced by Hill in [13], in the year 1948, and then later modified into other forms like Hill79, Hill90 and Hill93.

In addition to the Hill family of models, which are derived from quadratic form, exists a family of models based on crystal plasticity. These models are generally based on Hosford yield criterion [14], which was proposed with the crystallographic structure in mind. One of the most commonly used models in metal forming with regards to this family is the Yld89 criterion [15] by Barlat. This model provides relatively high accuracy for aluminum alloys with minimal anisotropy. However, it has notable limitations, including inaccurate predictions of biaxial yield strength [1]. Furthermore, while only four coefficients are required (and one chosen according to the crystallographic structure of the material), these coefficients lack any direct physical meaning.

Following this work, Barlat and Banabic proposed advanced versions of this criterion. Barlat created a 3D extension for the model in Yld91 criterion [16] and Banabic proposed extensions of this criterion to seven and eight coefficients in BBC (Banabic-Balan-Comsa) criteria. The Yld91 was later expanded to Yld94 and Yld96 that were more general and more suitable for aluminum alloys, that were becoming increasingly popular. These criteria however, are very complex to the point that the convexity of yield functions is not guaranteed and the derivatives of equivalent stress are difficult to obtain analytically [1].

After the rise of advanced materials like dual phase steels and aluminum alloys having better properties, new yield criteria were forced to be developed. Into this group belongs the already mentioned BBC family of criteria, with the most popular BBC2005 model, commonly available in forming softwares like AutoForm, and the Barlat family of models into which belongs the Yld2004-18p, used in this research.

This thesis aims to compare Hill48 and Yld2004-18p anisotropic models and various approaches of YP determination in the case study of a cylindrical cup deep-drawing process. Both of these topics and their influence on the deep-drawing processes are widely discussed in the current literature. However, if the anisotropic models are compared in this example, the YP identification method (and consequently the Young's modulus determination interval) is often overlooked. The same holds vice-versa, studies on YP identification methods typically focus on specific directions of material, with limited consideration of broader applications.

The deep drawing cup test, also known as Swift test, is one of the most widely utilized and extensively studied methods for determining anisotropy during sheet metal forming. The experiment involves a circular sheet metal that is drawn into a die by a cylindrical punch, while its circumference is held by constant holding force. This test is generally described by the standard EN 1669. However, it provides very little information about the actual course of the test and instead focuses more on defining the geometry of individual parts of the setup. The final evaluation of anisotropy is then recommended by measuring so-called earing. After the complete drawing of the sheet, the resulting cup has varying height around its circumference.

2 Theoretical background

As mentioned, most of the current software tools still use the standard elasto-plastic material model where the total true strain $\boldsymbol{\varepsilon}$ is defined by

$$\boldsymbol{\varepsilon} = \boldsymbol{\varepsilon_e} + \boldsymbol{\varepsilon_p}, \tag{1}$$

where $\boldsymbol{\varepsilon}$ is the tensor of total true strain and $\boldsymbol{\varepsilon_e}$ and $\boldsymbol{\varepsilon_p}$ are the elastic and plastic components, respectively. Of course this model predicts an instantaneous yield point, where plastic deformation starts to manifest itself alongside the elastic deformation. Elastic strain is then described by Hooke's law, which assumes linear relationship between stress and strain:

$$\boldsymbol{\sigma} = \mathbf{E} : \boldsymbol{\varepsilon_e}, \tag{2}$$

where $\boldsymbol{\sigma}$ is the stress tensor and $\mathbf{E}$ is the fourth-order tensor of elastic constants. On the other hand, plastic strain of advanced materials with hardening can be described with various hardening models, such as linear strain hardening, Ludwik, Swift-Voce, etc.

2.1 Determination of yield point

The plastic strain in the case of uniaxial tension is determined by subtracting the elastic (linear) component from the total strain such as

$$\varepsilon^p = \varepsilon - \frac{\sigma}{E}, \tag{3}$$

where ε is total true strain, ε^p is the true plastic strain, σ is true stress and E is Young's modulus. Identifying the upper boundary of the elastic region for Young's modulus determination is, for the purposes of this study, equivalent to determining the yield point (YP) of the material. The corresponding true stress value at this point is referred to as the yield strength. This is due to the overall reduction in variability of experimental data, which would be higher if E were calculated first and then true plastic strain of 0 derived from it.

According to ISO 6892-1, the upper boundary for determining the Young's modulus E is defined as half of the offset yield strength at 0.2% plastic strain. Therefore, for the purposes of this work, 50% of this offset yield strength will be used as the YP, where the plastic strain is considered zero.

The method developed by Merklein in [8], applied in this study, has also been utilized in previous research in case of biaxial stress state, as reported in [17]. This method identifies the end of the elastic region from the true stress - true strain curve by calculating the energy density under the curve. It employs two different computational approaches, one of which aligns more closely with the linear part of the curve while the second one is more general. The YP is then determined as the point where the results from the two computational methods begin to diverge.

In this study however, the main focus was on the determination of YP depending on temperature of the specimen. At first, temperature declines since the volume of the continuum under approximately adiabatic conditions is rising according to the equation

$$\Delta \mathrm{T} = \frac{\alpha \mathrm{T} \Delta \sigma}{\rho \mathrm{c}_p}, \tag{4}$$

where ΔT is the temperature change, T is the current temperature, α is the coefficient of linear thermal expansion, $\Delta\sigma$ is stress change, ρ is material density and c_p specific heat capacity at constant stress. As described by Thomson in [18], this holds true even for solid elastic materials and is used in [9].

The plastic deformation energy, on the other hand, is dissipated as heat at a rate of 85-95%, following a nonlinear relationship [11, 12]. During the uniaxial uniform loading of tensile test specimen, the temperature therefore follows curve such as in Fig. 1. At first, the deformation is elastic and therefore the temperature declines roughly linearly, then after the YP of the material is reached, the temperature starts to rise as plastic deformation manifests alongside the elastic part. At the minimum of the temperature curve, the two energies from elastic and plastic deformation are in balance and therefore the YP has to lie before the point of minimum [9].

Because of this, the first derivative of the temperature curve should be partly approximately constant transitioning into almost linear slope and the second derivative should see a spike in the transition area where YP is to be expected. These principles were studied by Volk in [9, 19], leading to the development of a range of methods aimed at accurately deriving these transitions from noisy signals. In this work, efforts were made to apply two of these methods. The first method fits two lines on the first derivative at the start and near the minimum of temperature signal [9]. The YP is predicted where the two lines intersect. The second method uses second order regularization and considers the maximum a YP. This was deemed to be the most robust approach in [19]. The measurement data in these articles however, are quite precise or artificially generated and the methods mentioned are therefore not robust enough for appropriate use in this study despite these efforts.

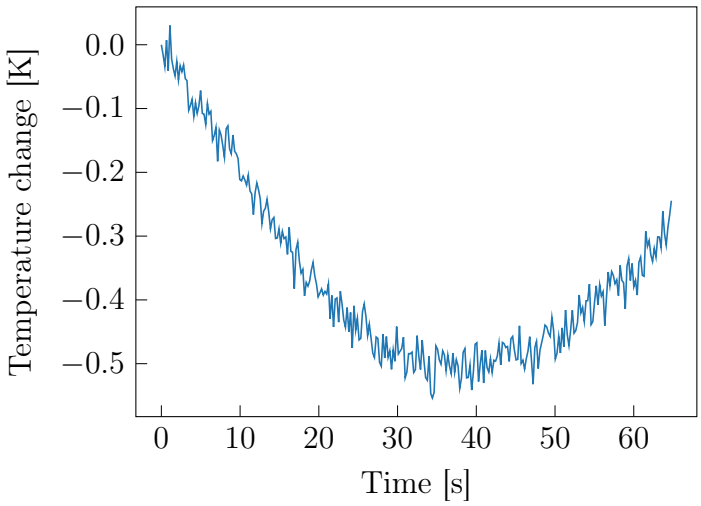

Fig. 1: Temperature change during uniaxial quasi-static loading

Because of this, simultaneously with this study in collaboration with the thesis supervisor Zajíček, a novel approach for determining the onset of yielding is being developed. The results of this work are currently being prepared for publication. Unlike derivative based approaches, this one operates directly on the original data, making them appear more robust to noise.

The method relies on a piecewise approximation of the experimental data using quadratic functions. The YP of the specimen is then identified based on the minimum length of the curve. Specifically, the YP corresponds to the intersection of the tangent line drawn from the origin and the tangent line at the point of the minimal curve length.

The final temperature-based method studied remains the identification of the minimum of the temperature signal. This approach is the most robust and proves highly effective even in the presence of significant noise, as it does not require any additional signal processing. For example, in [20], a thermal camera was used to monitor the temperature, and the detected minimum was within approximately 5% of the YP for the aluminum alloy under investigation.

2.2 Anisotropy models in metal forming

The anisotropic properties are usually described by various yield surface models. The classical model for anisotropic materials is the quadratic form created by Mises in [21]. The quadratic formula is the anisotropic extension of the von Mises isotropic model and has the following shape:

$$\begin{aligned}\Phi = {} & h_{11}\sigma_{11}^2 + h_{22}\sigma_{22}^2 + h_{33}\sigma_{33}^2 + h_{44}\sigma_{12}^2 + h_{55}\sigma_{23}^2 + h_{66}\sigma_{31}^2 + \\ & + 2h_{12}\sigma_{11}\sigma_{22} + 2h_{13}\sigma_{11}\sigma_{33} + 2h_{14}\sigma_{11}\sigma_{12} + 2h_{15}\sigma_{11}\sigma_{23} + \\ & + 2h_{16}\sigma_{11}\sigma_{31} + 2h_{23}\sigma_{22}\sigma_{33} + 2h_{24}\sigma_{22}\sigma_{12} + 2h_{25}\sigma_{22}\sigma_{23} + \\ & + 2h_{26}\sigma_{22}\sigma_{31} + 2h_{34}\sigma_{33}\sigma_{12} + 2h_{35}\sigma_{33}\sigma_{23} + 2h_{36}\sigma_{33}\sigma_{31} + \\ & + 2h_{45}\sigma_{12}\sigma_{23} + 2h_{46}\sigma_{12}\sigma_{31} + 2h_{56}\sigma_{23}\sigma_{31},\end{aligned} \tag{5}$$

where σ_{ij} are the respective components of the Cauchy stress tensor and h_{ij} are constant.

From this model Hill created a simplified criterion alongside with various other models as was already mentioned. The Hill48 model [13] will be the main representative of this family of models in this thesis for its simplicity.

Barlat's Yld2004-18p model, on the other hand, is one of the advanced yield criteria developed to accurately predict the behavior of advanced materials [1]. The criterion itself is isotropic with respect to its parameters, but these parameters depend on the material's anisotropy. The model was developed based on the Hosford criterion [14], which is expressed as

$$f(\sigma_{ij}) = F|\sigma_{22} - \sigma_{33}|^m + G|\sigma_{33} - \sigma_{11}|^m + H|\sigma_{11} - \sigma_{22}|^m, \tag{6}$$

The exponent m is determined by the crystallographic structure of the material. For materials with Body-Centered Cubic structure (including DP1000 used in this study), $m = 6$, while for materials with Face-Centered Cubic structure, $m = 8$. Based on the Hosford model, the Yld89 and other criteria were developed. Yld2004-18p model will be used in this study because of its complexity and ability to accurately predict anisotropic behavior.

2.2.1 Model Hill48

One of the first anisotropic models, based on the quadratic form, described by Eq. (5), created by Hill in [13] introduces the yield criterion in the form

$$\begin{aligned}2f(\sigma_{ij}) = {} & F(\sigma_{22} - \sigma_{33})^2 + G(\sigma_{33} - \sigma_{11})^2 + H(\sigma_{11} - \sigma_{22})^2 + \\ & + 2L\sigma_{23}^2 + 2M\sigma_{31}^2 + 2N\sigma_{12}^2 = 1,\end{aligned} \tag{7}$$

where F, G, H, L, M, N are constant coefficients characteristic of the current state anisotropy. This criterion in this form relies on the fact that the principal axes of anisotropy are chosen as axes of reference. In the case of sheet metals, the rolling direction is usually parallel to axis 1, the transverse direction axis 2, and the direction along the thickness of the sheet axis 3.

If plane stress conditions are considered in the plane $\sigma_{\widehat{11}\sigma_{22}}$, the criterion (7) simplifies to the following form:

$$2f(\sigma_{ij}) = (G+H)\sigma_{11}^2 - 2H\sigma_{11}\sigma_{22} + (H+F)\sigma_{22}^2 + 2N\sigma_{12}^2 = 1. \tag{8}$$

If tensile yield strengths in the principal directions are introduced as X, Y, Z, along with shear yield strength in the $\sigma_{\widehat{11}\sigma_{22}}$ as T, the coefficients used in Eq. (8) can be expressed from Eq. (7) as:

$$\begin{aligned} \frac{1}{X^2} &= G+H, \qquad \frac{1}{Y^2} = H+F, \\ \frac{1}{Z^2} &= F+G, \qquad \frac{1}{T^2} = 2N. \end{aligned} \tag{9}$$

If the yield values are then introduced into Eq. (8), the model takes the form of

$$\frac{1}{X^2}\sigma_{11}^2 - (\frac{1}{X^2} + \frac{1}{Y^2} - \frac{1}{Z^2})\sigma_1\sigma_2 + \frac{1}{Y^2}\sigma_{22}^2 + \frac{1}{T^2}\sigma_{12}^2 = 1. \tag{10}$$

When the principal directions of the stress tensor coincide with the principal anisotropic axes, the criterion reduces by the shear component into form

$$\frac{1}{X^2}\sigma_1^2 - (\frac{1}{X^2} + \frac{1}{Y^2} - \frac{1}{Z^2})\sigma_1\sigma_2 + \frac{1}{Y^2}\sigma_2^2 = 1, \tag{11}$$

where σ_1, σ_2 are the principal stresses.

In Abaqus documentation [22], the Hill48 anisotropic criterion is described differently, using the potential function

$$f(\sigma_{ij}) = \sqrt{\begin{array}{c} F(\sigma_{22}-\sigma_{33})^2 + G(\sigma_{33}-\sigma_{11})^2 + H(\sigma_{11}-\sigma_{22})^2 + \\ +2L\sigma_{23}^2 + 2M\sigma_{31}^2 + 2N\sigma_{12}^2 \end{array}}, \tag{12}$$

resulting in the plane stress version of the criterion in the form

$$f(\sigma_{ij}) = \sqrt{F(\sigma_{22}-\sigma_{33})^2 + G(\sigma_{33}-\sigma_{11})^2 + H(\sigma_{11}-\sigma_{22})^2 + 2N\sigma_{12}^2}, \tag{13}$$

which is similar to Eq. (8), but the coefficients are defined as follows:

$$\begin{aligned} F &= \frac{\sigma_0^2}{2}\left(\frac{1}{Y^2} + \frac{1}{Z^2} - \frac{1}{X^2}\right) = \frac{1}{2}\left(\frac{1}{R_{22}^2} + \frac{1}{R_{33}^2} - \frac{1}{R_{11}^2}\right), \\ G &= \frac{\sigma_0^2}{2}\left(\frac{1}{Z^2} + \frac{1}{X^2} - \frac{1}{Y^2}\right) = \frac{1}{2}\left(\frac{1}{R_{33}^2} + \frac{1}{R_{11}^2} - \frac{1}{R_{22}^2}\right), \\ H &= \frac{\sigma_0^2}{2}\left(\frac{1}{X^2} + \frac{1}{Y^2} - \frac{1}{Z^2}\right) = \frac{1}{2}\left(\frac{1}{R_{11}^2} + \frac{1}{R_{22}^2} - \frac{1}{R_{33}^2}\right), \\ N &= \frac{3}{2}\left(\frac{\tau_0}{\sigma_{12}}\right)^2 = \frac{3}{2R_{12}^2}, \end{aligned} \tag{14}$$

where σ_0 is the user-defined reference yield strength, R_{ij} are anisotropic yield strength ratios with respect to σ_0 and $\tau_0 = \sigma_0/\sqrt{3}$. The associated flow rule is incorporated from Lévy-Mises equations as

$$d\boldsymbol{\varepsilon}^p = d\lambda \frac{\partial f}{\partial \boldsymbol{\sigma}} = \frac{d\lambda}{f}\boldsymbol{b}, \tag{15}$$

where dλ is the hardening parameter, $d\boldsymbol{\varepsilon}^p$ is the increment of plastic strain, and from Eq. (12) the $\boldsymbol{b}$ has the form

$$\boldsymbol{b} = \begin{bmatrix} -G(\sigma_{33} - \sigma_{11}) + H(\sigma_{11} - \sigma_{22}) \\ F(\sigma_{22} - \sigma_{33}) - H(\sigma_{11} - \sigma_{22}) \\ -F(\sigma_{22} - \sigma_{33}) + G(\sigma_{33} - \sigma_{11}) \\ 2N\sigma_{12} \\ 2M\sigma_{31} \\ 2L\sigma_{23} \end{bmatrix}. \tag{16}$$

This approach is basically the same, except to create a von Mises criterion in Eq. (7) the coefficients necessary are $F = G = H = 1$ and $L = M = N = 3$, while in Abaqus Eq. (12), the coefficients needed are $F = G = H = 0.5$ and $L = M = N = 1.5$.

For sheet metals, the standard procedure involves conducting uniaxial tension tests at three orientations ($\theta = 0°$, $45°$, and $90°$, where θ is the angle of the specimen relative to the rolling direction of the sheet), as well as a bulge test to induce a equibiaxial tension state. Alternatively, a cross specimen can be used to achieve biaxial tension, or a stack test for compression in the thickness direction. These tests enable the measurement of anisotropy through two variations: strain anisotropy, characterized by Lankford coefficient (r_θ), or yield strength anisotropy ($\tilde{\sigma}_\theta$).

While yield strength of the specimen is self explanatory, the Lankford coefficient (r-value) is defined as a ratio of true plastic strain across specimen width ε_w^p to that through the thickness ε_t^p like so:

$$r = \frac{\varepsilon_w^p}{\varepsilon_t^p}. \tag{17}$$

With this in mind, it is possible to define two versions of Hill48 criterion Hill48σ and Hill48r. During the construction of Hill48σ, the yiled stress values are used to determine the coefficients in Eq. (8) or Eq. (13). For the yield strength values from uniaxial tensile tests cut at an angle θ from rolling direction of the sheet, the stress state is as follows

$$\sigma_{11} = \tilde{\sigma}_\theta cos^2(\theta) \qquad \sigma_{22} = \tilde{\sigma}_\theta sin^2(\theta) \qquad \sigma_{12} = \tilde{\sigma}_\theta cos(\theta) sin(\theta), \tag{18}$$

where $\tilde{\sigma}_\theta$ is the yield strength of the specimen, see [23]. Therefore, $\tilde{\sigma}_0$ and $\tilde{\sigma}_{90}$ are X and Y values respectively, and $\tilde{\sigma}_{45}$ is determined for the coefficient N, where, if Eq. (18) for $\theta = 45°$ is substituted into Eq. (13), the coefficient N can be described as in [24]

$$N = \frac{\sigma_0^2}{2}\left(\frac{2}{\tilde{\sigma}_{45}^2} - \frac{1}{Z^2}\right), \tag{19}$$

or, if substituted into Eq. (8) as in [25]

$$N = \frac{1}{2}\left(\frac{4}{\tilde{\sigma}_{45}^2} - \frac{1}{Z^2}\right). \tag{20}$$

The yield strength Z can be directly determined through a stack test, which compresses the material along its thickness direction. However, as discussed in [26], it can be replaced by the equibiaxial yield strength, $\tilde{\sigma}_b$, since plastic flow is governed by the deviatoric component of the Cauchy stress tensor. This component remains identical under equibiaxial tension and uniaxial compression. Since $\tilde{\sigma}_b$ is easier to determine, it is commonly used in most studies. If only uniaxial tension tests are conducted, the yield strength Z can be estimated as the mean value of the in-plane yield strengths

$$Z = \frac{1}{4}(\tilde{\sigma}_0 + 2\tilde{\sigma}_{45} + \tilde{\sigma}_{90}), \tag{21}$$

as proposed by Volk in [25]. However, this approach can be inaccurate.

The r-values are introduced into the criterion through the plastic deformation, for which the associated flow rule, described by Eq. (15), can be used with respect for the Hill48 criterion. After introducing Eq. (18) into Eq. (8) and accounting for Eq. (15), the following applies:

$$\begin{aligned} d\varepsilon^p_{11} &= [(G+H)cos^2\theta - Hsin^2\theta]\sigma_\theta d\lambda, \\ d\varepsilon^p_{22} &= [(F+H)sin^2\theta - Hcos^2\theta]\sigma_\theta d\lambda, \\ d\varepsilon^p_{33} &= -(Fsin^2\theta + Gcos^2\theta)\sigma_\theta d\lambda, \\ d\gamma^p_{12} &= (Nsin\theta cos\theta)\sigma_\theta d\lambda. \end{aligned} \tag{22}$$

where σ_θ is the true stress in the specimen. The r-value of the specimen, defined by Eq. (17), can be therefore described as

$$\begin{aligned} r_\theta &= \frac{d\varepsilon^p_{11}sin^2\theta + d\varepsilon^p_{22}cos^2\theta - 2d\gamma^p_{12}sin\theta cos\theta}{d\varepsilon^p_{33}} = \\ &= \frac{H + (2N - F - G - 4H)sin^2\theta cos^2\theta}{Fsin^2\theta + Gcos^2\theta}, \end{aligned} \tag{23}$$

as mentioned in [23], and the coefficients from Eq. (8) are described as in [27], with the use of $\theta = 45°$ specimen and additional proposition, that $G + H = 1$:

$$\begin{aligned} F &= \frac{r_0}{(1+r_0)r_{90}}, \qquad G = \frac{1}{1+r_0}, \\ H &= \frac{r_0}{1+r_0}, \qquad N = \frac{(r_0+r_{90})(2r_{45}+1)}{2r_{90}(1+r_0)}. \end{aligned} \tag{24}$$

This is also shown in [1]. Alternatively for the version used in Abaqus, represented by Eq. (13), where the additional equation is described as $R_{11} = 1$, and the coefficients can be calculated using

$$\begin{aligned} R_{11} = 1, \qquad R_{22} &= \sqrt{\frac{r_{90}(r_0+1)}{r_0(r_{90}+1)}}, \qquad R_{33} = \sqrt{\frac{r_{90}(r_0+1)}{r_0+r_{90}}}, \\ R_{12} &= \sqrt{\frac{3r_{90}(r_0+1)}{(2r_{45}+1)+(r_0+r_{90})}}, \end{aligned} \tag{25}$$

as mentioned in [28]. This model constructed using the Lankford coefficients is usually referred to as Hill48r. The Hill model defined in [27] then predicts the equibiaxial yield

strength and r-value as

$$\tilde{\sigma}_b = \frac{\tilde{\sigma}_0}{\sqrt{F+G}}, \qquad r_b = \frac{F}{G}. \tag{26}$$

The Hill48r model is mathematically equivalent to Hill48σ when the associative flow rule is considered. However, the deformation-based approach results in different coefficients. The r-value is primarily determined in the plastic region of the flow curve, as it is typically measured between 5–20% elongation [29], if feasible. In this study, for DP1000 steel, the r-value was measured from 2% plastic strain up to the start of necking. Consequently, this approach yields different coefficients compared to direct yield strength determination.

To mitigate the difference between these two approaches, an optimization method was developed [27], which minimizes the error function

$$\begin{aligned} Error\_fcn = w_1 \sum_{i=1}^{n} \left(\frac{(\tilde{\sigma}_\theta)_{\text{pred}} - (\tilde{\sigma}_\theta)_{\text{exp}}}{(\tilde{\sigma}_\theta)_{\text{exp}}} \right)_i^2 + w_2 \sum_{i=1}^{n} \left(\frac{(r_\theta)_{\text{pred}} - (r_\theta)_{\text{exp}}}{(r_\theta)_{\text{exp}}} \right)_i^2 + \\ + w_3 \left(\frac{(\tilde{\sigma}_b)_{\text{pred}} - (\tilde{\sigma}_b)_{\text{exp}}}{(\tilde{\sigma}_b)_{\text{exp}}} \right)^2 + w_4 \left(\frac{(r_b)_{\text{pred}} - (r_b)_{\text{exp}}}{(r_b)_{\text{exp}}} \right)^2, \end{aligned} \tag{27}$$

where w_i are the predetermined weight coefficients, n is the number of measured data points, $()_{\text{pred}}$ represents the values predicted by the Hill criterion, and $()_{\text{exp}}$ are the corresponding experimental values. To minimize this function, the Sequential Least Squares Programming (SLSQP) method was employed, with the initial iteration chosen using coefficients that define the von Mises criterion. This optimized version is referred to as Hill48*opt*.

2.2.2 Model Yld2004-18p

The Yld2004-18p criterion, introduced in [30], is a three-dimensional extension of earlier planar anisotropy models and is expressed as follows:

$$\Phi(\tilde{\boldsymbol{S}}', \tilde{\boldsymbol{S}}'') = |\tilde{S}_i' - \tilde{S}_j''|^m, \qquad f(\sigma_{ij}) = \sqrt[m]{\frac{\Phi(\tilde{\boldsymbol{S}}', \tilde{\boldsymbol{S}}'')}{4}}, \tag{28}$$

where m has the same significance as in Hosford model and is based on crystallographic structure of the material, $\tilde{S}_i$ and $\tilde{S}_j$ are the principal values of $\tilde{\boldsymbol{S}}'$ and $\tilde{\boldsymbol{S}}''$, which are first and second linear transformations of the deviatoric stress tensor $\boldsymbol{S}$. The deviatoric stress vector $\hat{\boldsymbol{S}}$ is obtained and transformed by

$$\begin{aligned} \widehat{\tilde{\boldsymbol{S}}'} &= \boldsymbol{C}'\hat{\boldsymbol{S}} = \boldsymbol{C}'\boldsymbol{T}\hat{\boldsymbol{\sigma}}, \\ \widehat{\tilde{\boldsymbol{S}}''} &= \boldsymbol{C}''\hat{\boldsymbol{S}} = \boldsymbol{C}''\boldsymbol{T}\hat{\boldsymbol{\sigma}}, \end{aligned} \tag{29}$$

where $\boldsymbol{T}$ transforms the stress vector $\hat{\boldsymbol{\sigma}}$ to deviatoric stress vector $\hat{\boldsymbol{S}}$, and $\widehat{\tilde{\boldsymbol{S}}'}$ and $\widehat{\tilde{\boldsymbol{S}}''}$ are the first and second linear transformations of the stress vector. The tensors are then directly derived. The transformation matrix is defined as

$$\boldsymbol{T} = \frac{1}{3} \begin{bmatrix} 2 & -1 & -1 & 0 & 0 & 0 \\ -1 & 2 & -1 & 0 & 0 & 0 \\ -1 & -1 & 2 & 0 & 0 & 0 \\ 0 & 0 & 0 & 3 & 0 & 0 \\ 0 & 0 & 0 & 0 & 3 & 0 \\ 0 & 0 & 0 & 0 & 0 & 3 \end{bmatrix}, \tag{30}$$

and the first and second linear transformations on the stress deviator have the shape

$$\boldsymbol{C^*} = \begin{bmatrix} 0 & -c_{12}^* & -c_{13}^* & 0 & 0 & 0 \\ -c_{21}^* & 0 & -c_{23}^* & 0 & 0 & 0 \\ -c_{31}^* & -c_{32}^* & 0 & 0 & 0 & 0 \\ 0 & 0 & 0 & c_{44}^* & 0 & 0 \\ 0 & 0 & 0 & 0 & c_{55}^* & 0 \\ 0 & 0 & 0 & 0 & 0 & c_{66}^* \end{bmatrix}, \tag{31}$$

where symbol $\boldsymbol{C^*}$ replaces $\boldsymbol{C'}$ or $\boldsymbol{C''}$, and symbol c_{ij}^* replaces c_{ij}' or c_{ij}'' for first or second linear transformation respectively. However, in Abaqus, the transformation matrix components are annotated differently, and the values of c_{44}^*,c_{55}^* and c_{66}^* are divided by 2.

When $m = 2$ or $m = 4$, and all the coefficients c_{ij}' and c_{ij}'' are equal to 1, the yield function reduces to the von Mises criterion. Conversely, for $m = 0$ or $m \to \infty$, it simplifies to the Tresca criterion. Furthermore, when $\boldsymbol{C'} = \boldsymbol{C''}$, meaning the formulation accounts for only a single linear transformation, it reduces to Yld91 [31]. The predicted yield strength values for this criterion can be computed using Eq. (28), by substituting the corresponding stress states given in Eq. (18):

$$\tilde{\sigma}_\theta = \sqrt[m]{\frac{\Phi(\sigma_{11}, \sigma_{22}, \sigma_{12})}{4}}, \tag{32}$$

which can be found in [32], and the predicted r-value is then calculated as mentioned in [33]:

$$r_\theta = \frac{sin\theta cos\theta \frac{\partial f}{\partial \sigma_{12}} - sin^2\theta \frac{\partial f}{\partial \sigma_{11}} - cos^2\theta \frac{\partial f}{\partial \sigma_{22}}}{\frac{\partial f}{\partial \sigma_{11}} + \frac{\partial f}{\partial \sigma_{22}}}. \tag{33}$$

With these values, it is possible to introduce error function, formulated in [30], for optimizing the components of $\boldsymbol{C'}$ and $\boldsymbol{C''}$:

$$Error\_fcn = \sum w_\sigma \left(\frac{(\tilde{\sigma}_\theta)_{pred}}{(\tilde{\sigma}_\theta)_{ex}} - 1 \right)^2 + \sum w_r \left(\frac{(r_\theta)_{pred}}{(r_\theta)_{ex}} - 1 \right)^2, \tag{34}$$

where w_σ and w_r are the weight coefficients for stress and deformation anisotropy, respectively. These values must be predetermined, see [33, 30], and are typically chosen as $w_\sigma = 1$ and $w_r = 0.1$.

As previously outlined, the experiments required for this criterion include uniaxial tensile tests conducted at angles $\theta \in \{0°, 15°, 30°, 45°, 60°, 75°, 90°\}$. Additionally, the values $\tilde{\sigma}_b$ and r_b from other experiments can be incorporated. Furthermore, four additional data points characterizing out-of-plane properties are required. These values can be extracted from crystallographic texture. however, it is also possible to assume isotropic material behavior in the thickness direction [30].

2.3 Deep drawing circular cup test

The deep drawing cup test is one of the possible experiments for determination of anisotropy during metal sheet forming. For the purposes of this thesis, it was used to demonstrate the accuracy of the models and methods of YP determination mentioned

above. The setup for this test is illustrated in Fig. 2. During the test, the punch moves quasi-statically into the sheet with a constant velocity, forming the sheet into a cup shape via the die. The resulting cup height is then measured. If the material is isotropic, the height remains uniform around the circumference. However, if the material is anisotropic, the cup height will vary depending on the angle from the rolling direction of the sheet.

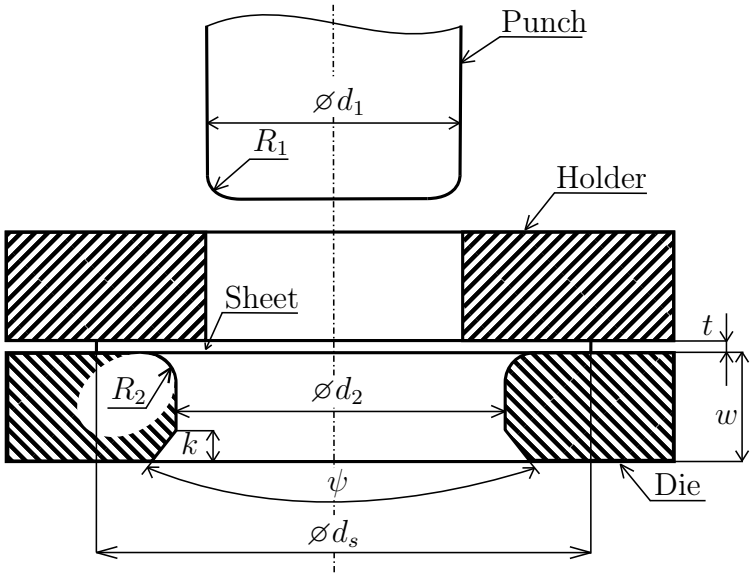

Fig. 2: Experimental setup used in deep drawing cup test

The multi-center study [34] was conducted on the topic of this experiment and compared the different approaches of its simulation on the example of AA 6016-T4 aluminum alloy. One key comparison parameter is the force generated by the punch during the drawing process. Not only to verify the correct course of the experiment, but also to determine the friction coefficient to be used in numerical models. The typical relation between force and punch displacement is shown in Fig. 3.

The force amplitude will be naturally dependent on the material used. However, as is described in [34], the force curve can be typically divided into 4 segments. The first phase is the bending of the material, during which its stiffness increases against the punch. This is followed by a phase where a significant portion of the material is already outside the blank holder, resulting in less resistance and a decrease in force. Next comes the ironing phase, which occurs due to the material's greater or same thickness than the clearance between the punch and the die. The material is compressed into this clearance, distributing its thickness more evenly, while the system's stiffness remains relatively unchanged. The final phase is earing, where the curve stabilizes again because some parts of the material are already fully shaped, while others still offer resistance. This phenomenon occurs only in the presence of material anisotropy.

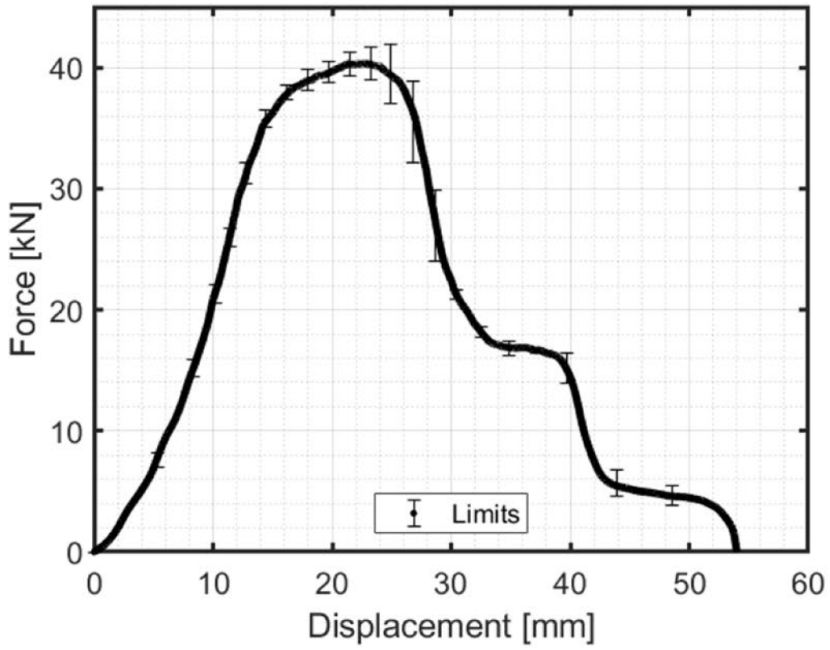

Fig. 3: Typical force development on the punch during cup test (drawn from [34])

Another way to verify the accuracy of the model is by analyzing the thickness distribution of the material along the line connecting the center of the sheet to its edge. Naturally, this distribution will vary depending on the material and, in the case of anisotropy, also on the direction. However, in general, the thickness profile should resemble the one shown in Fig. 4. Thickness is also primarily measured based on the rotation angle of the cup, which helps examine the material's anisotropy.

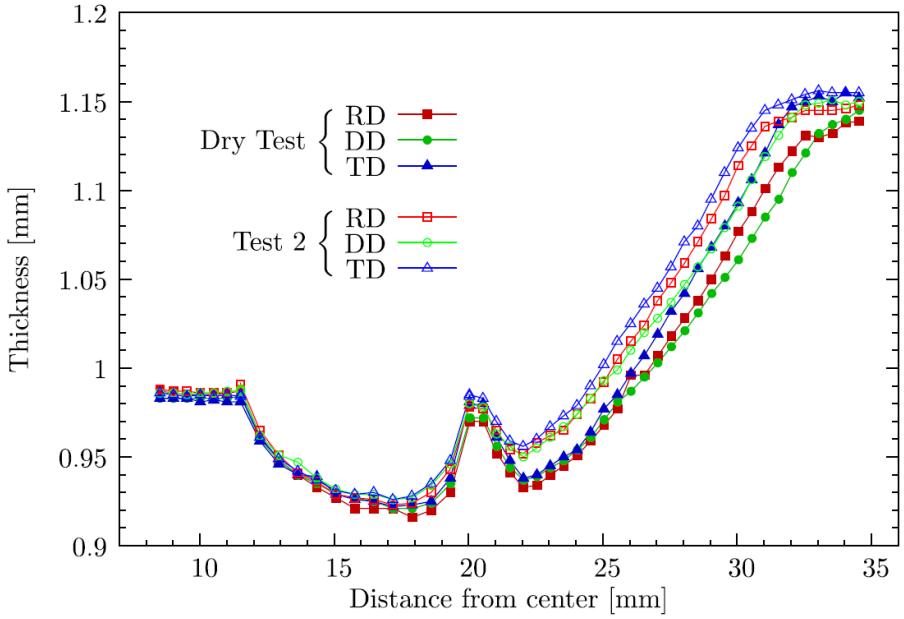

Fig. 4: Typical thickness distribution of the sheet along the line connecting the center to the edge after the test (drawn from [35])

For this study, a pre-existing device and pre-manufactured samples were used with resemblance of setup introduced in standard EN 1669, with addition of the relief (k and ψ) to easily extract the formed specimen. Consequently, the test does not fully conform to the EN 1669 standard, particularly the condition $d_2 - d_1 < 2t$. The dimensions used for the setup in this study are introduced in table 1.

Variable	Dimension
d_1	100 mm
d_2	103 mm
d_s	150 mm
R_1	10 mm
R_2	10 mm
t	0.8 mm
w	60 mm
k	25 mm
ψ	30°

Table 1: Dimensions used in deep drawing cup test setup in Fig. 2

The results of this experiment however, rely greatly on the dimensions of the setup. The study [36] proves, that it is possible to simply annulate the earing of the cup by introducing a non uniform clearance between the punch and die. This clearly shows that clearance has a severe influence on the result of the experiment. Since increased clearance causes greater specimen bending and reduces the effectiveness of the ironing phase, detecting anisotropy becomes more challenging.

Additionally, the standard does not specify the punch fillet radius R_1 for punch diameters other than 33 mm or 50 mm. However, in this case, R_1 is directly proportional to the value specified for a 50 mm punch diameter. Similarly, the die fillet radius R_2 is only recommended for punch diameters of 33 mm and 50 mm, with no guidance for other values. As noted in study [37], the radii R_1 and R_2 used in the testing setup influence the final results. Nevertheless, the radii used in the experiments seem as viable options given the EN 1669 standard, despite not being explicitly specified for the different punch diameter. Additionally, the sheet diameter d_s does not conform to the standard. As a result, the experiments cannot be considered fully compliant with this standard, the current setup is suboptimal, and it is recommended to follow the prescribed dimensions for future experiments.

3 Performed experiments

As previously stated, the studied material was a dual phase high strength steel DP1000. Its chemical and metallographic properties were studied in COMTES FHT a.s. and were provided by the company for the needs of this thesis for complete information about the material. The chemical composition of this material is described in table 2.

C [%]	Fe [%]	Si [%]	Mn [%]	Cr [%]
0.166	96.28	0.168	2.273	0.497
P [%]	Ni [%]	Cu [%]	Nb [%]	Al [%]
0.013	0.018	0.015	0.023	0.053

Table 2: Chemical composition of studied material

To ensure the correct orientation of the sheet and subsequently all samples, every sample was marked accordingly. The RD was then determined from a metallographic examination in Fig. 5. The section was carved from a formed cup in the TD and the perpendicular RD is clearly visible.

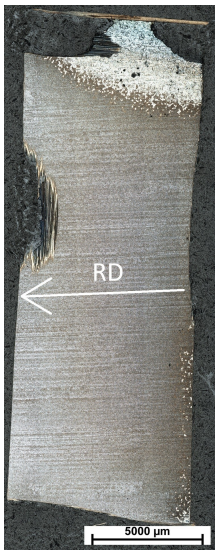

(a) Metallographic section

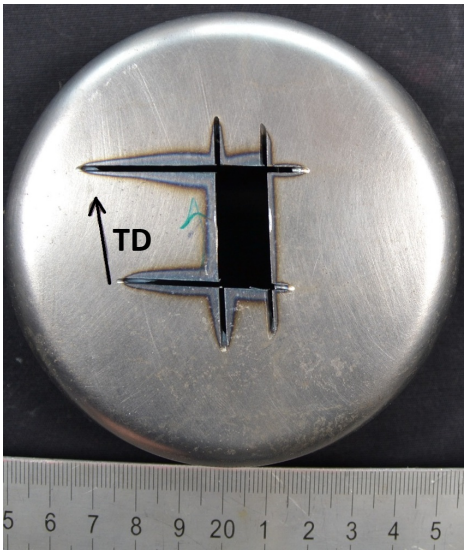

(b) Orientation of the section based on the formed cup

Fig. 5: Metallographic section for RD confirmation

To calibrate the material model, uniaxial tensile tests were conducted to determine the elasto-plastic properties of DP1000. A total of 21 dog-bone-shaped specimens (with middle section 90 mm × 20 mm), 0.8 mm thick, were tested, with three samples taken at every 15° interval from the rolling direction (RD) to the transverse direction (TD). This sampling approach effectively supports the calibration of the Yld2004-18p criterion. However, three specimens were excluded due to inconsistencies. The testing procedure involved a load velocity of 0.75 mm/min up to 1.5 mm elongation to capture detailed yield onset behavior, followed by an increase to 3 mm/min until failure for r-value calculation.

Deep drawing experiments were conducted using 10 circular specimens. However, due to ongoing refinements in the cup experiment setup, which had not been previously used for this purpose, only four specimens contributed to the final analysis. The punch velocity was set at 30 mm/min until the fully formed cup was released from the die, which happens after about 75 mm of punch displacement. The sheet was held with approximately 112 kN of force, which was determined by earlier simplified simulations to be sufficient, and the sheet therefore did not wave during the experiment.

3.1 Performed uniaxial tensile tests

YP and Young's modulus for each specimen were determined using various methods outlined in Chapter 2.1, along with the corresponding r-value. The r-value was calculated following the EN ISO 10113 standard, which requires Young's modulus to determine the specimen's true plastic strain. The variation in r-value across different Young's modulus determination methods was marginal compared to the variation across different specimens. Therefore, a single r-value was calculated for each specimen using the Young's modulus value, that was found according to the standard ISO 6892-1.

The tensile tests were performed at room temperature, without temperature control, with both deformation measurement and temperature measurement, as demonstrated in Fig. 6. The deformation of the specimen was measured using the ARAMIS DIC system, while the temperature was monitored with three K-type thermocouples insulated with ceramic wool to isolate the area near the measurement point. Because of the lack of further stabilization of the surrounding temperature and the type of thermal couples used, the temperature signal contained a severe amount of noise. Most of the current methods for YP determination however, were not developed on noisy data and lack the necessary robustness. To use these methods, a new approach of data approximation was developed as mentioned in Chapter 2.1.

(a) Setup from the deformation measurement side

(b) Setup from the thermal measurement side

Fig. 6: Setup for uniaxial tensile tests

The DIC measurement included three virtual extensometers. The first, 80 mm long and aligned with the specimen axis, was used to generate the true strain–true stress flow curve. The second and third, each 18 mm long, were positioned at the specimen's midsection—one along the axis of the specimen and the other perpendicular to it—to calculate the r-values.

Temperature measurements were obtained using three 0.2 mm Class K thermocouples placed along the longitudinal specimen axis—one at the center of the specimen and the others positioned at ± 1.5 mm from the center. This setup was inspired by study [38], which investigated the impact of thermocouple placement. However, it is likely that similar results could be achieved with a single thermocouple. While alternative attachment methods, such as the clip-on technique described in [9], can minimize interaction with the test sample, this study employed spot welding with 1 J of energy, leading to only surface-level distortions. Given the quasi-static nature of all tests, the potential for interference with the results was considered minimal. Additionally, to account for heat generated by the DIC system's lighting, each specimen was allowed to stabilize before measurements were taken.

In addition to the uniaxial tensile test, two biaxial tensile tests were conducted in an effort to obtain a more comprehensive description of the yield loci as in the previous research [17]. Although temperature measurements are clearly possible, as demonstrated in [39, 40] using 'full' cross specimens, they did not perform as expected in this study and the results are therefore not included. This discrepancy is attributed to localized plastic deformation occurring outside the uniform measurement area of the cross sample as samples with slits were used for more homogeneous stress distribution [41, 42]. Due to this localized deformation, heat may be conducted into the measurement area, potentially leading to inaccurate temperature readings.

3.2 Performed deep drawing circular cup test

The deep drawing circular cup test was conducted to validate the anisotropic models derived from uniaxial tensile tests on a unified forming process. The uniaxial test samples were taken from the same sheet as the circular samples, ensuring minimal material variation (as noted in [17], batch differences can significantly influence material properties). Although the test can be performed dry without lubrication, a standard oil, commonly used by PWO Czech Republic a.s., was applied to minimize friction-induced anisotropy. The holding force was set to approximately 110kN, although slight under-compensation during pressure regulation caused a minor increase during the experiments. However, this had only a negligible impact on the results. The test setup underwent iterative refinements, initially lacking sufficient coaxial accuracy.

To achieve proper alignment, particularly between the punch and die, a 3D-printed plastic ring was utilized, featuring an inner diameter matching the punch and an outer diameter matching the die. Before the experiment, the punch was extended into the die, pressing the ring into the clearance to distribute it evenly along the circumference. Additionally, small metal pieces were used to support the alignment pins, ensuring precise centering of the die and holder. And finally, a 3D-printed centering template was used to accurately fit the sheet into place. The use of the setup is shown in Fig. 7.

After the forming process, a 3D scanning system, ATOS, was employed to determine the overall shape of the drawn cups, as shown in Fig. 8. This is a non-destructive method

that can be used both to assess the earring of a cup and measure its thickness at various points. While the earring of the cup was relatively easy to measure with precision to tenths of a millimeter, the variation in thickness was only detectable in hundredths of a millimeter. Consequently, this measurement technique proved to be highly suitable, offering minimal potential for errors.

The orientation of the cup was defined by two small bumps located on the circumference of the circular sample, precisely in RD. These bumps served to fix the sample in place during the water jet cutting process. They were sufficiently distinct to enable orientation identification, yet small enough not to affect the subsequent forming process.

The cup forming process with eccentricity introduced a problem where the drawn cup's bottom was tilted. This caused the results to be unreliable, as the earing was not the dominant deformation, as shown in Fig. 9. Despite improvements to the setup to enhance its accuracy, eccentricity remained present. To address this, a simulation was conducted to confirm that mild eccentricity only caused the cup to appear tilted. With this confirmation, a curve of the form $a\ \sin\left(\frac{2\pi\theta}{360} + b\right) + c$ was subtracted from each cup height curve to eliminate the influence of the tilt. The coefficients a , b and c were optimized using the least squares method for each specimen.

(a) Testing device for deep drawing test

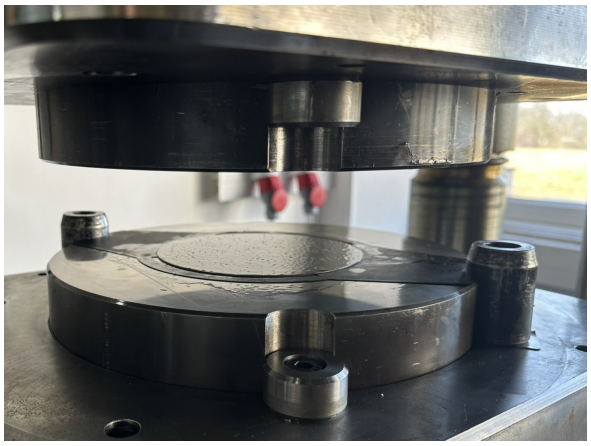

(b) Centering of test specimen using 3D-printed template

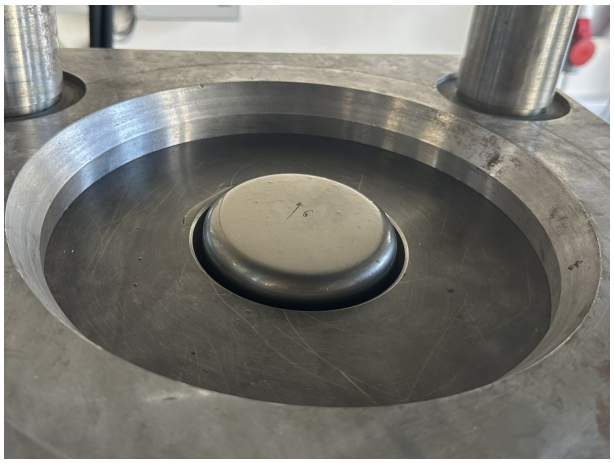

(c) Finished cup after the forming process

Fig. 7: Setup for the deep drawing cup test

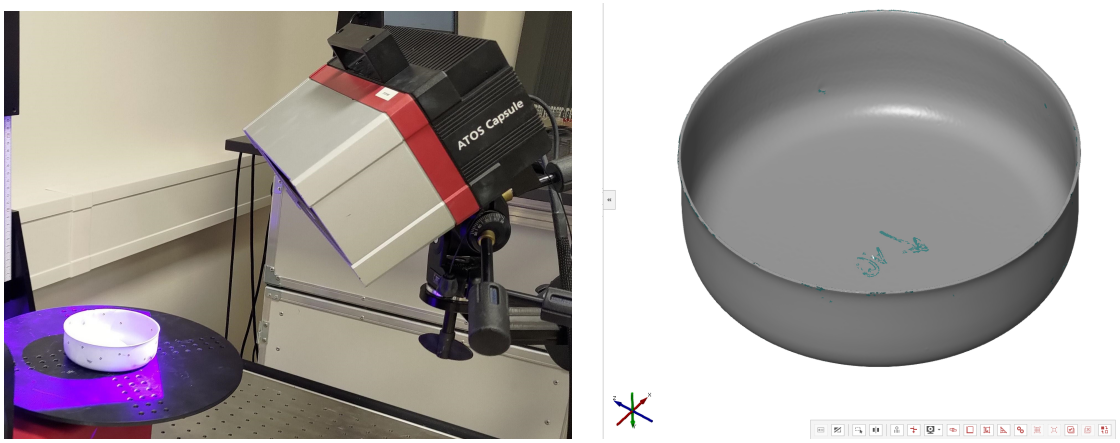

(a) Scanning of the formed cup (b) Scanned virtual model

Fig. 8: Scanning of a formed cup for determination of earing and thickness

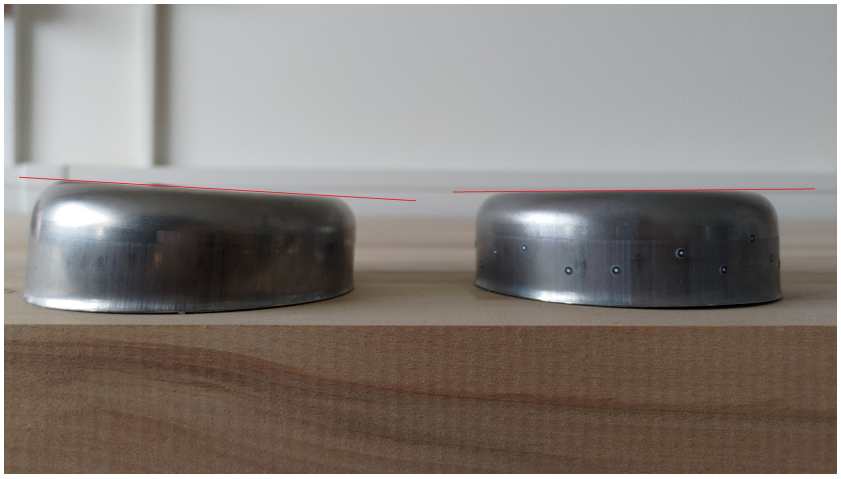

Fig. 9: The eccentricity problem creating tilted bottom of a cup (left) compared to a well formed cup (right)

3.3 Material models for FEA

Material models for the numerical simulations were developed mainly based on the results of uniaxial tensile tests. The YP for each specimen was determined using various methods in the effort to create the models as precise as possible. Some approaches relied solely on stress–strain data, while others primarily used temperature of the specimen as the key indicator. Subsequently, E was determined by linear regression over the interval between 5% of the point of loss of stability (start of necking) and the YP of the specimens in TD. An average value was then used for both YP and E. The flow curve was then shifted according to the offset of the linear fit to ensure that YP corresponded to 0% plastic strain, thereby maintaining continuity in the model. The true plastic strain - true stress data was considered up to the point of the loss of stability of the specimen.

For larger plastic deformations, one final point was added based on a Bulge test performed in previous research [43] and linearly extrapolated up to $\varepsilon^p = 1.5$, which is

demonstrated in Fig. 10. This flow curve is of course suboptimal, however since the only variable in the material models is type of YP determination method (influencing E thus also true plastic deformation calculated) and the anisotropy model used, the numerical results can be easily compared.

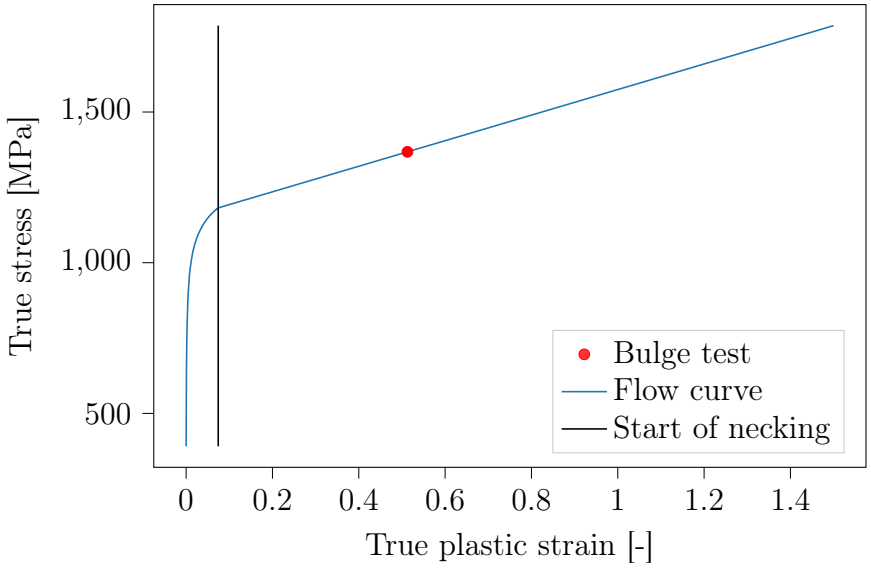

Fig. 10: Flow curve example

For each of the approaches of YP identification, a generalization can be made for DP1000 used in this study. The Merklein [8] method, that uses an incremental energy approach to determine the end of the linear part of strain-stress curve, usually generates lower values of yield strength since it does not assume any non-linear elastic behavior. The standard ISO 6892-1 does not specify the YP directly. It only gives an interval dependent on offset yield strength of 0.2% plastic strain leading to iterative determination of E and it's determination interval (10-50%). This results in very low variation since the relative difference of yield strength between the specimens is the same as at the offset yield strength, where the difference in stress is lower.

Most temperature-based methods introduced in recent literature proved to be highly inconsistent due to significant noise in the data. Even after extensive filtering and/or approximating the temperature curve by various means, these methods often failed to perform as intended, largely because they rely on the first and second derivatives of the temperature signal. In Fig. 11, the yield strength values obtained from these methods are compared with those from the newly developed approach, which does not utilize derivatives. It is evident that the method using the first derivative and line fitting onto it [9], generates yield strength that is often below 0 MPa (all values have been capped to be above 0) or unreasonably low. The maximum of 2nd regularization method, evaluated in [19] as the most reliable, generates YP often after temperature minimum, which is not the expected area of the YP as explained in Chapter 2.1. The temperature minimum approach and the newly developed approach, offered consistent and predictable results with relatively low variation. This is why the derivative dependent methods were excluded from further use in numerical models in this study.

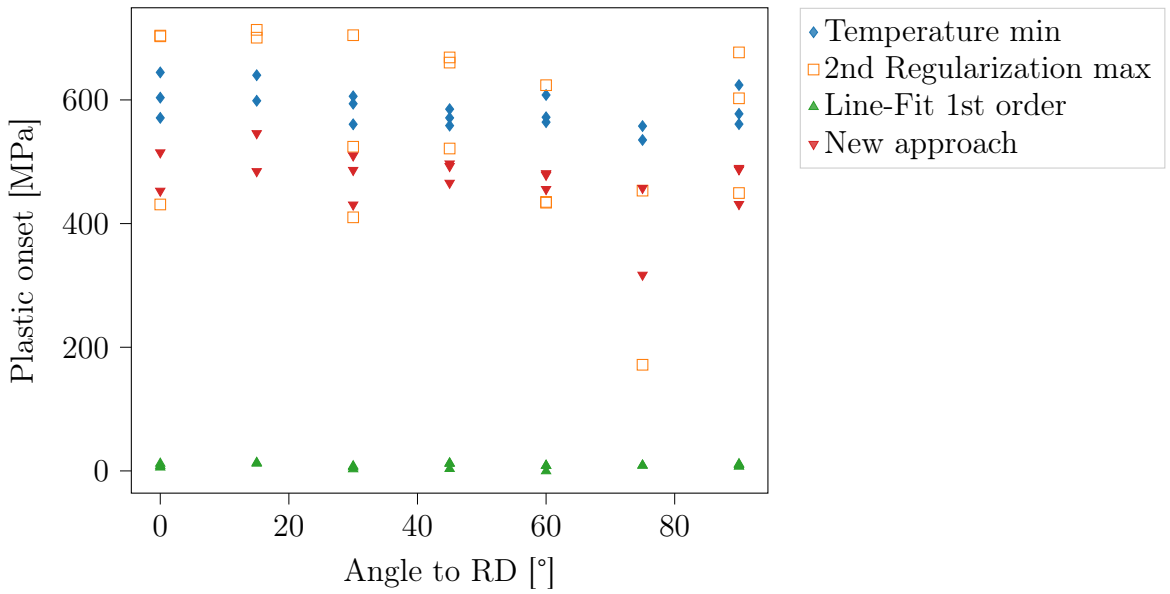

Fig. 11: Yield strength values obtained by different temperature methods

Since each of the methods used to determine the YP functioned differently, the values and the statistical distribution among specimens varied. Figure 12a presents the yield strength values obtained for each specimen using the various methods, highlighting that some methods exhibit a wider spread than others. The yield strength values were then averaged for specimens with the same orientation and the averaged results are shown in Fig. 12b.

If ISO 6892-1 is used, it generates values with remarkably low variation. This is due to the fact that 50% of the offset yield strength does not change the relative differences between the values, which is of course counter intuitive because the lower the deformation, the higher the spread in stress should be.

The temperature minimum produces values with higher spread than ISO 6892-1, however it is also very consistent and the variation is not high. Since it is easy to detect and does not rely on any additional signal manipulation, it is overall easy to employ and as it is clearly shown, is capable to detect anisotropy despite the variation. The newly developed approach has in general higher spread than the temperature minimum, but should yield more accurate predictions since in the time of minimal temperature plastic strain has to be present. The values of yield strength are higher than the values specified by ISO 6892-1 and lower than values detected by temperature minimum.

The method by Merklein [8] has the highest spread and lowest values with some of the specimens yielding below 200 MPa. The high variation resulted in the fact, that it is not entirely possible to detect the anisotropy of the material and the anisotropic coefficients could be impacted heavily by the data quality. A detailed table of these averages, along with the corresponding Young's modulus and calculated r-values, is provided in Appendix 1. The r-values are also illustrated in Fig. 12c, demonstrating a strong dependence on the specific specimen and only a minor influence from the YP determination method.

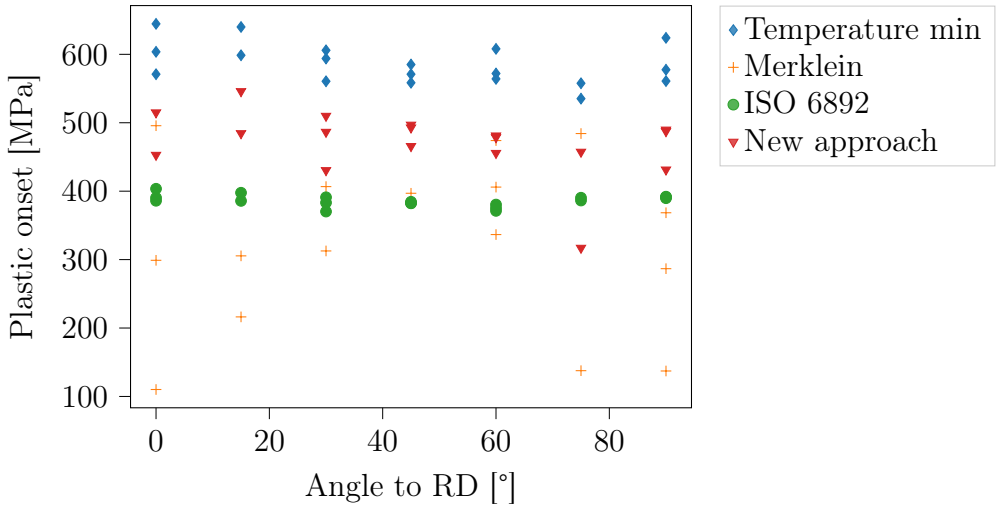

(a) Yield strength of all specimens

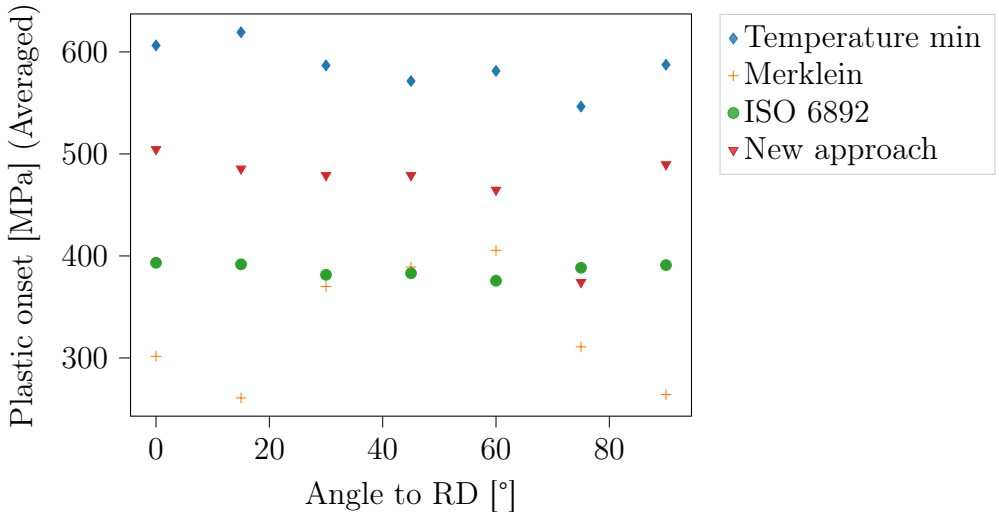

(b) Averaged yield strength for each orientation

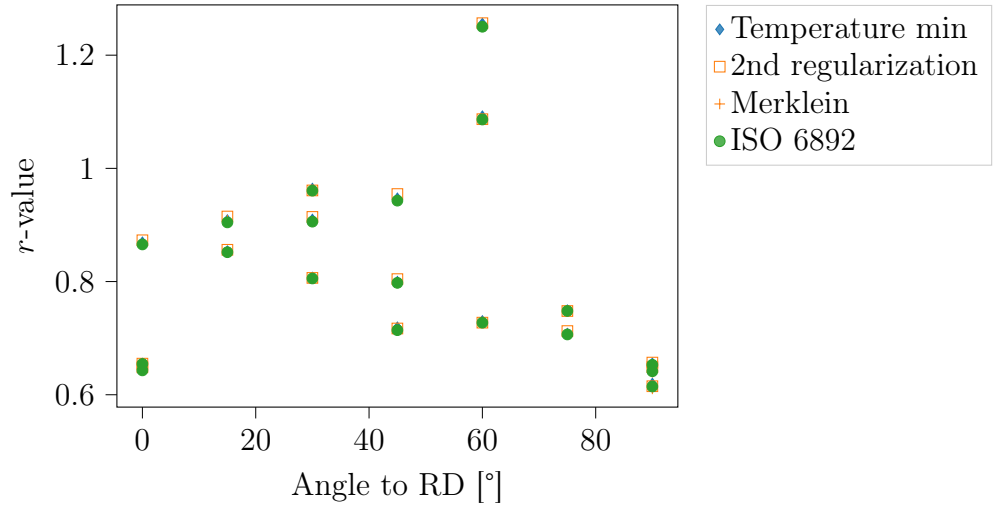

(c) r-values dependence on YP determination method

Fig. 12: Summary of yield strength and r-value behavior based on YP determination method used

Using all available yield strength and r-value data, an Abaqus plug-in *Anisotropy Calculator* [44] was employed to calculate the coefficients required for both anisotropic yield criteria. This plug-in implements each of the theoretical coefficient determination methods described in Chapter 2.2. All methods, except one, rely solely on uniaxial tensile test data. However, the Hill48σ formulation additionally requires the equibiaxial yield strength. Although this value can be estimated from various sources, the method proposed by Volk [25] (see (21)) was used in this work to use purely the uniaxial tensile test data.

The various anisotropic models, calibrated according to the YP determination as specified by ISO 6892-1, are presented in Fig. 13. It is evident that the Hill48r model predicts the r-values in RD, DD and TD perfectly while Hill48σ model predicts the yield strength values. From the predicted yield strength values, it is also clear that the anisotropy of Hill48σ model will be the mildest.

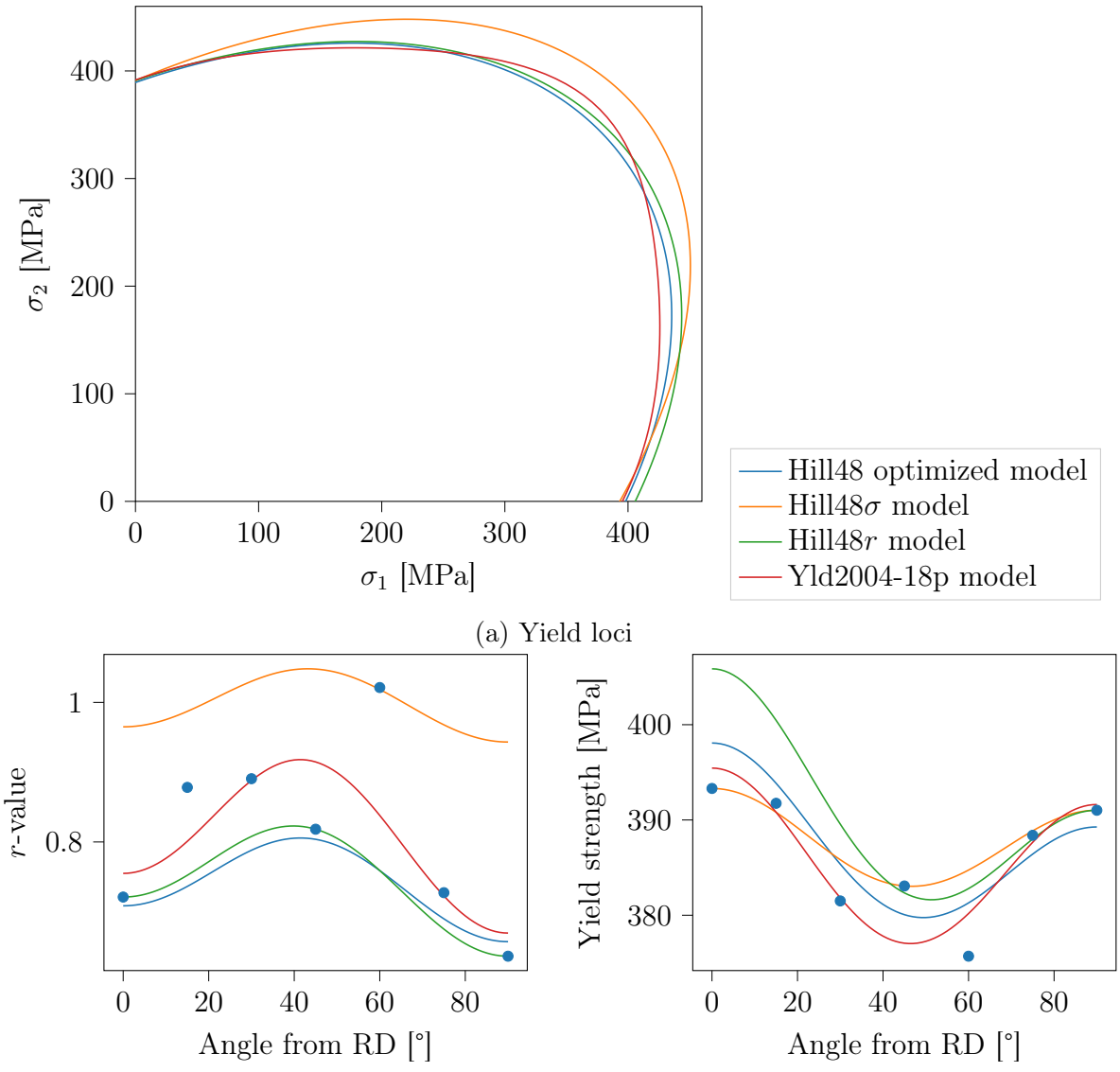

(a) Yield loci

(b) Difference in r-value

(c) Difference in yield strength value

Fig. 13: Anisotropic models with experimental data evaluated according to ISO 6892-1

The Hill48r and Hill48σ models coincide at the yield strength in the TD, with the Hill48σ model generally exhibiting higher stress values on the yield loci. Despite the weight of r-values in the error function being set to 0.1 compared to 1 for the yield strength values, the more complex Hill48*opt* model tends to follow more the Hill48r model. It also no longer respects the yield strength in TD. The most advanced model, Yld2004-18p, incorporates all the experimental data and therefore attempts to minimize the error in every direction. Due to its non-quadratic nature, with a parameter value of $m = 6$ in (28), it is capable of representing a more complex yield locus shape.

As was already mentioned, the r-values from the experiments were almost non dependent on the YP determination method used. That is because they rely only very mildly on E, which is used to calculate ε^p. The Hill48r criterion is therefore only dependent on the yield strength in TD and the anisotropy character does not change much. This can be easily proven by comparing two yield loci of Hill48r constrained to a single yield strength in TD in Fig. 14. From this is clear that the differences in anisotropy coefficients between the different YP determination methods for this model are negligible and only shift with the single value of yield strength in TD.

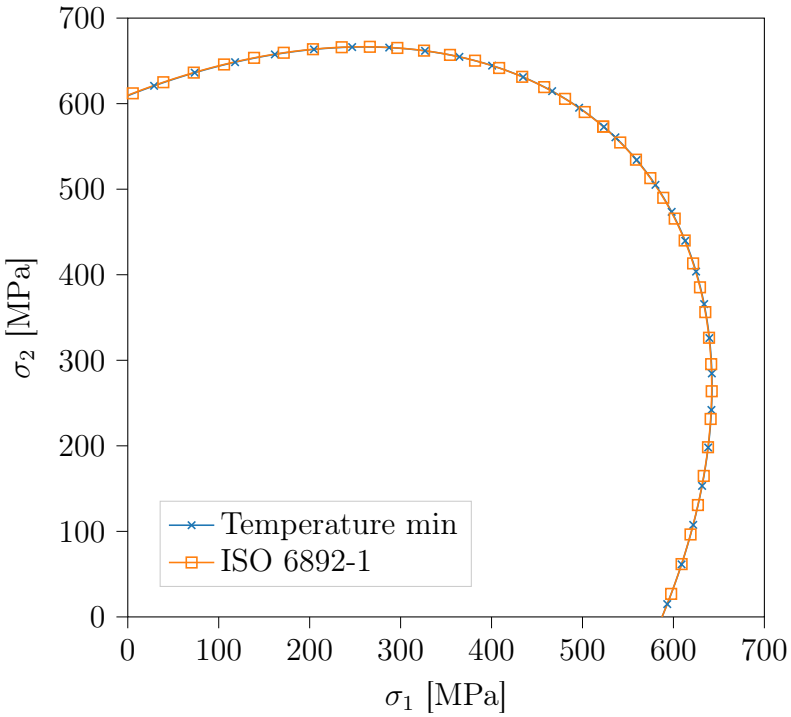

Fig. 14: Two Hill48r models constrained to a single yield strength in TD

4 FE model of deep drawing cup test

The finite element model for the cup forming simulations was developed using Abaqus FEM software. In Abaqus, two main models were created. One using the Hill48 anisotropic criterion, where SC8R (continuum shell) elements were used with two symmetry planes and one using the Yld2004-18p criterion with C3D8R and C3D8I (3D stress) elements utilizing half of the domain. The continuum shell or any conventional shell elements in Abaqus do not offer the option to use this criterion. The simulations were made using Abaqus/Explicit solver with Abaqus/Standard (implicit static solver) used for the simulation of springback. Because the holding force during the experiments was not constant, it was introduced into the model as an experimental curve, that was measured with empty machine setup to match the experiments.

All objects, except for the sheet, were modeled as analytical rigid bodies. Alternatively, they can be modeled as discrete rigid bodies, which slightly increases the analysis time and may introduce minor surface discontinuities, leading to negligible contact vibrations. However, testing simulations confirmed that this approach is generally acceptable and does not significantly affect the simulation results. The total punch displacement was set to 45 mm and applied using a Smooth Step amplitude profile, which was also used to apply the initial holding force prior to the onset of the drawing process.

The contact was defined as 'hard' in the normal direction, with Coulomb friction set to 0.17 to approximately match the force amplitude observed in the experiments, as observed in the current literature [34, 35]. Due to the presence of rigid bodies, a penalty contact formulation with default settings was employed to ensure more stable simulation. All interactions were modeled using surface-to-surface contact with a finite sliding formulation. Given the use of the explicit solver, default contact controls were applied and there was no need for numerical damping of the contact. To prevent the holder from moving above the die level, a wire feature was used in combination with a stop command, triggered once the holder was fully in contact with the die.

For each model, a corresponding springback simulation was performed. This simulation served exclusively to release the formed cup, with boundary conditions applied by constraining central node of the cup's mesh. This approach allowed the springback process to be treated as a static problem and was solved using the Abaqus/Standard solver. Consequently, issues related to vibrations or other dynamic phenomena were avoided, and since the deformation was purely elastic, the springback was resolved within a single computational step.

After the springback, a vertical coordinate of the outer edge of the sheet was analyzed to assess the earing of the cup. The simulation results were processed in the same manner as the experimental results, and the cup height was measured from the central point of the cup (which remained fixed during the springback). Due to the use of explicit solver in previous (forming) step, the vertical coordinate of this fixed node was different for each model and, due to the mild anisotropy, played a role in the resulting cup height measurement. To compensate for a slight tilt of the cup after the explicit solving process the data were corrected using the formula $a\ \sin\left(\frac{2\pi\theta}{360} + b\right) + c$ fitted onto each earing profile, the same way as to experimental values. The amplitude however, was of course, orders of magnitude lower.

4.1 Solver choice and non-physical model settings

Initially, a simplified model was developed in Marc/Mentat 2014 using a static implicit simulation. However, Marc/Mentat 2014 does not natively support the Yld2004-18p yield criterion and is considered outdated. Moreover, for potential future developments, such as the inclusion of failure modeling, Abaqus/Explicit was selected as the preferred tool for similar forming problems. Abaqus/Standard is unsuitable for such applications, as it cannot effectively handle the very large strains involved and, according to the Abaqus documentation [22], is highly inefficient for forming simulations.

Although the cup test can be simulated using an implicit solver, in Abaqus this requires the implementation of normal direction contact control. This method introduces numerical static damping into the model, making it essential to verify that the added energy does not influence the overall simulation results. A similar consideration applies to Abaqus/Explicit, where careful monitoring of the model's kinetic energy (ALLKE) is necessary. Specifically, the ALLKE should remain below 2–5% of the stored elastic strain energy (ALLSE) to ensure simulation accuracy [22]. However, managing ALLKE in explicit simulations is generally easier than controlling contact-induced damping in implicit analyses, as it can be reduced by increasing the total simulation time. The total time of the forming step was chosen as 0.06 s, which means, that it was comfortably above the necessary 0.0269 s threshold, given by the inverted value of ten times the first eigenfrequency of the sheet, recommended in [22].

However, despite this, for all models, ALLKE did not consistently remain below the recommended threshold, often peaking at up to 30% of ALLSE. These peaks, however, were caused by the sudden release of the sheet from the holder during forming. The more isotropic the material behavior, the higher the observed peak. This resulted in vibrations in the force response at the moment of sheet release. Nevertheless, since these vibrations did not affect the plastic deformation of the sheet and were not excessively severe, it was concluded that this behavior is acceptable and does not compromise the simulation results (final form of the cup), particularly for anisotropic materials.

As previously mentioned, it is necessary to monitor ALLKE during explicit simulations. However, there are additional important aspects to ensure the physical accuracy of the simulation. One of the most critical is the use of mass scaling. Mass scaling slightly increases the mass of small, targeted elements to allow larger stable time increments for the explicit solver. Since this introduces non-physical behavior, it is essential to monitor the resulting changes in the model's mass [22]. If the target time increment is set too large, the model's mass may change substantially, leading to inaccurate simulation results.

The last non-physical behavior affecting the model is the hourglass effect. This phenomenon occurs when under-integrated elements, typically reduced integration elements often used in explicit analyses, distort into an hourglass shape without providing any resistance to this deformation. This can be improved by two methods, mesh refinement or stabilization.

If smaller elements are used, the distortion of said elements is lower and therefore the hourglass effect is mitigated. This however, can play a role in the computational cost. Abaqus therefore offers several stabilization methods to control this behavior. These methods mostly work by changing the stiffness of the element, but since that change is not physically based, it introduces 'artificial strain energy' into the model. This artificial energy (ALLAE) must be carefully monitored and should not exceed 5% of ALLSE to maintain the physical accuracy of the simulation [22].

4.2 Deep drawing cup test simulation using Hill48 criterion

For the simulation using the Hill48 yield criterion, a shell model was employed. Specifically, SC8R (continuum shell) elements were used. These elements have eight nodes with only three degrees of freedom per node while employing the kinematics of shell elements [22]. Due to this configuration, the elements can be stacked through the thickness of the sheet. Their reduced integration makes them well-suited for large deformation simulations using an explicit solver. However, this same feature can lead to stability issues, particularly facing collapse due to hourglass effect.

The suitability of these elements for the problem at hand is thoroughly discussed in [35], where the SC8R element type is compared to the C3D8I element. The study clearly demonstrates that, although SC8R elements offer a less precise representation of the final cup thickness, they accurately predict the earing profile while significantly improving computational efficiency. Additionally, it is shown that the number of integration points through the thickness of the shell element has a minimal impact on the overall results. However, it should be noted that the study utilized only a single SC8R element through the thickness and 3 C3D8I elements. As previously mentioned, continuum shell elements have the advantage of allowing multiple layers, which can lead to a more accurate prediction of material thinning. Therefore, using more than one element across the thickness may enhance the accuracy of thinning prediction.

Two models were developed in total: one representing the full geometry of the sheet, and another exploiting symmetry by modeling only a quarter of the sheet with two symmetry planes along the principal axes. Quarter model consisted of 31330 elements while the full model had 105049 elements, specific mesh and assembly configuration can be seen in Fig. 15. Both models performed as expected, with ALLAE amounting to approximately 1.4% of ALLSE, using only one element across the thickness of the sheet while a default hourglass control setting was used for the material models tested.

The two models exhibited slightly different behaviors. To compare the earing effects, both isotropic and anisotropic cups were simulated, as illustrated in Fig. 16. The simulation results clearly indicate that when isotropic material properties are assumed, the relative error between the two models is significantly higher. In contrast, incorporating anisotropy reduces the numerical relative errors to a negligible level. Consequently, all Hill48 models were simulated with two symmetry planes, as the absolute error in earing resulting from numerical inaccuracies was approximately 0.004 mm.

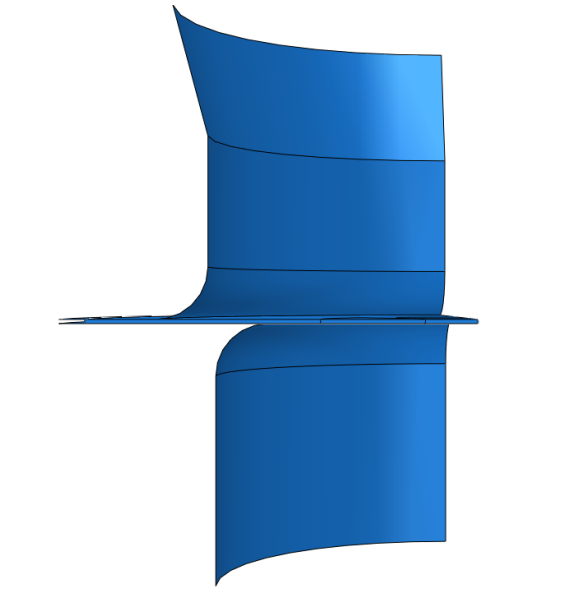

(a) Assembly with two symmetry planes

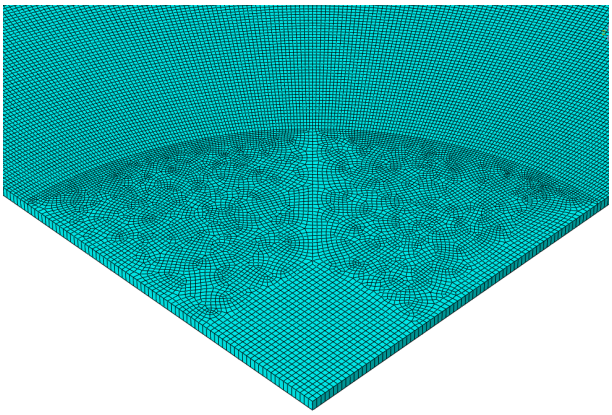

(b) Detail of mesh of the shell model

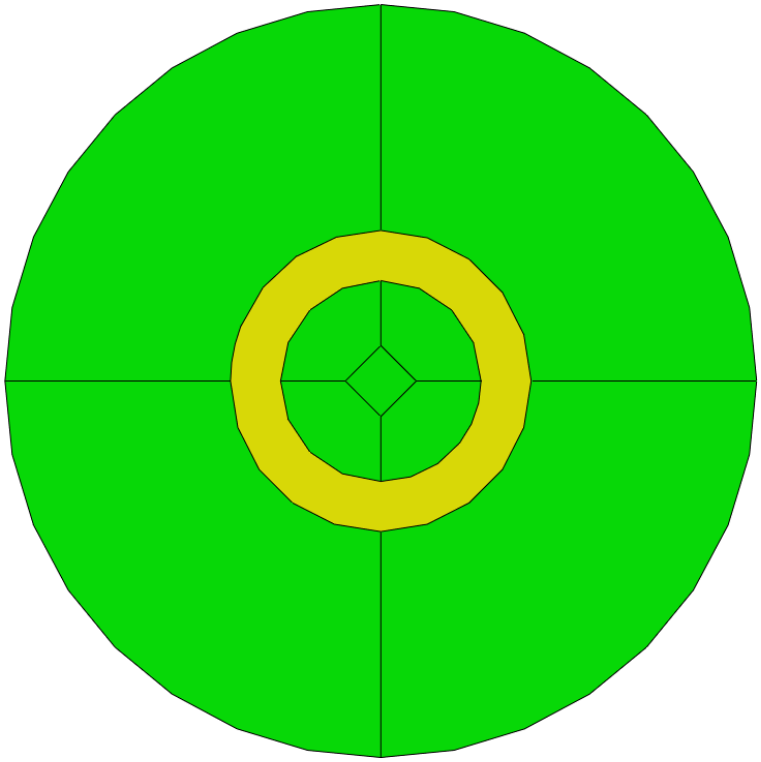

(c) Sections for mesh control - structured mesh in green, advancing front in yellow

Fig. 15: Structure of mesh of models used to simulate Hill48 criterion

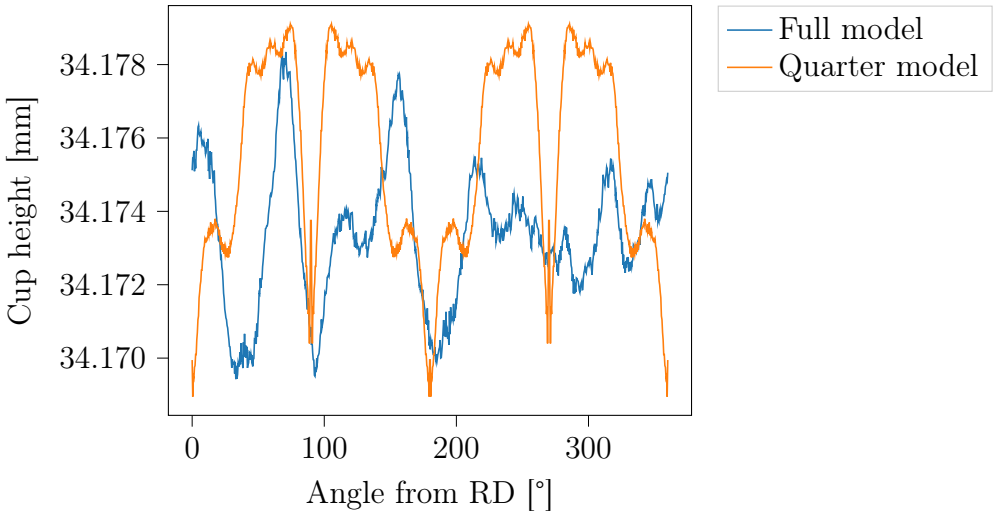

(a) Isotropic cup height

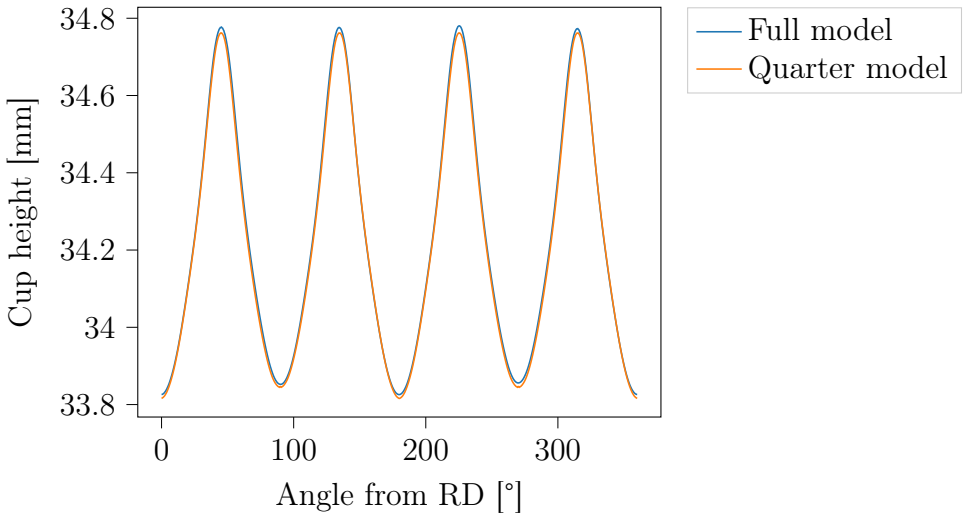

(b) Anisotropic cup height

Fig. 16: Difference of cup height between full and quarter sheet simulation

The smallest, critical element had a stable time increment of 1.67×10^{-8} s. To enhance computational efficiency, mass scaling was applied, increasing the time increment to 4×10^{-8} s for elements with a stable time increment below this threshold. The overall change in the model's mass was approximately 0.251%, which is negligible considering the significant reduction in computational time.

4.3 Deep drawing cup test simulation using Yld2004-18p criterion

For the simulation using the Yld2004-18p criterion, a full-domain model should be employed, as the criterion does not possess any axis of anisotropic symmetry. However, after the experimental cup measurement (results in the following chapter), the cup height appeared to be symmetrical with one axis of symmetry. Therefore, model utilizing one half of the circular sheet was used. Additionally, since only 3D element types in Abaqus support

this anisotropic criterion, the model required a large number of elements, in particular 125582, because of the necessity to use multiple element layers, resulting in significantly increased computational time.

Two types of elements were used in this model: C3D8I and C3D8R. Since C3D8R elements with reduced integration often lose stability under bending, C3D8I elements, recommended in [35], with specially formulated incompatible modes, were preferred in regions experiencing significant deformation. The main downside of this element is that it is fully integrated, which can be very cost inefficient for explicit analysis. The remaining areas of the sheet, particularly the central region subjected to minimal deformation, were therefore meshed using C3D8R elements to improve computational efficiency. The mesh with the element type used is demonstrated in Fig. 17. Due to the full integration of C3D8I elements, only 2 element layers were used for the simulation.

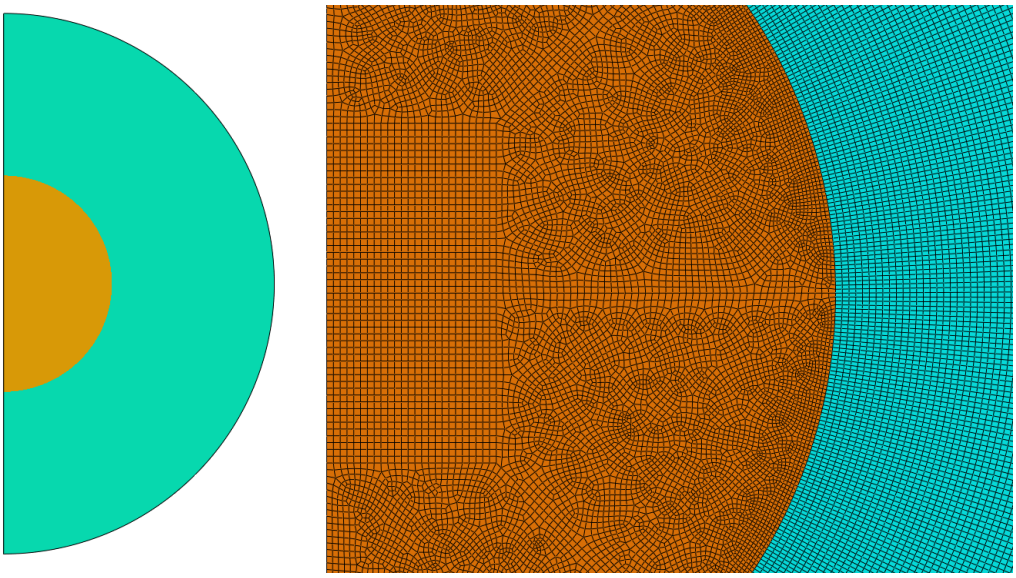

(a) Element type of the 3D model

(b) Detail of mesh of the 3D model

Fig. 17: Mesh and element type of 3D model - C3D8I in blue, C3D8R in orange

The smallest, critical element had a stable time increment of 1.47×10^{-8} s with mass scaling applied to increase the time increment to 3×10^{-8} s for elements with a stable time increment below this threshold. The overall change in the model's mass was approximately 0.1%.

Although the model utilized the Relax Stiffness option for hourglass control of the C3D8R elements, the ALLAE remained below 0.1% of ALLSE, indicating that its effect was negligible. This was because the deformation in the central area was very small and thus the C3D8R elements were not unstable. In contrast, when only C3D8R elements were used in the whole domain with five elements through the thickness (resulting in higher number of integration points through the thickness), the ALLAE increased to as much as 50% of ALLSE. This led to non-physical behavior, compromising the reliability of the results. For physically accurate results, an even higher number of elements would have to be used.

5 Comparison of FE models and experimental results

The friction level in the models was determined from the experimental force curve, as previously mentioned. There was minimal variation in the force curves across different specimens apart from one. Therefore, an average curve was used for comparison with the model results, as shown in Fig. 18. Because the device does not directly measure the force on the punch, but the overall force including the holding force, an empty test without a sheet was once performed to obtain a force curve (used as a holding force for the models) that was then subtracted to obtain the final value of force caused by the sheet itself. The force curves of the isotropic and anisotropic models were very similar. However, the isotropic model exhibited more pronounced vibrations due to the sudden release of the sheet from the holder in the explicit simulation as expected.

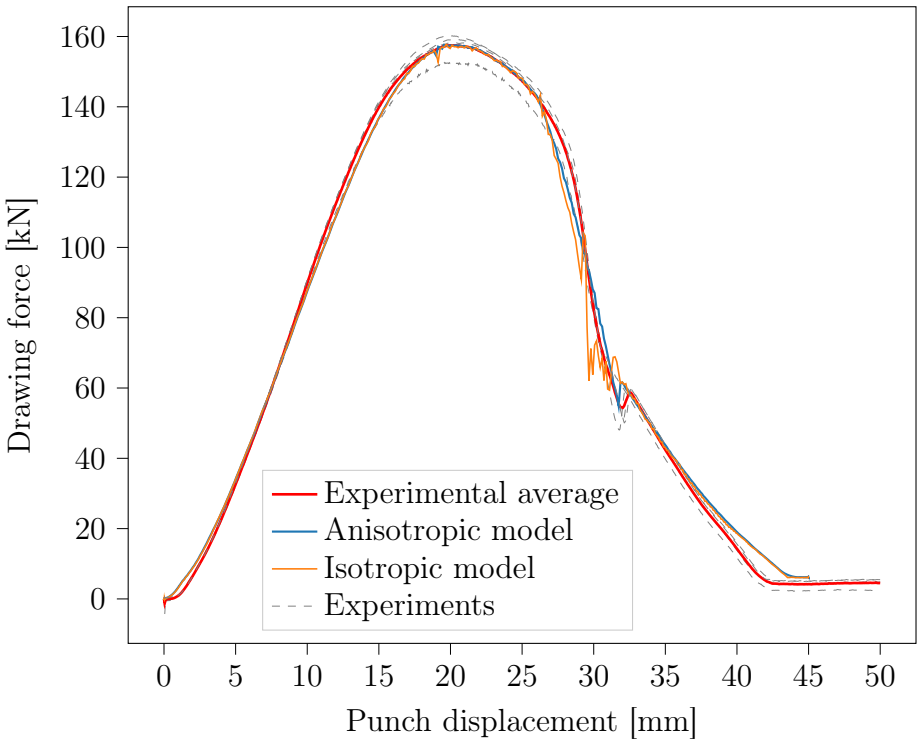

Fig. 18: Force development during cup test

It is also worth noting that the overall shape of the force curve closely resembles the typical profile found in the literature (see Fig. 3), despite the testing setup not adhering strictly to standard specifications. The main difference lies in the greater clearance between the die and punch, which resulted in the absence of an ironing phase, which normally helps to even out material thickness and make earing more noticeable. Consequently, had the test been performed in full compliance with the standard, more pronounced earing might have been observed, making it easier to measure and evaluate the results.

Another way to validate the overall suitability of the performed tests and the model used is through the measurement of cup thickness. The thickness distribution along the RD, DD, and TD directions, as shown in Fig. 19, exhibited minimal variation with respect to orientation and demonstrated a similar pattern to that reported in the literature (Fig. 4). This consistency suggests that the experimental setup is reliable and unlikely to produce misleading results.

Isotropic shell and 3D models were also included for comparison. Although the predicted values from these models are generally lower than the measured ones, this discrepancy is likely due to the fact that the experimental sheets had an average initial thickness of 0.809 mm, whereas a value of 0.8 mm was used in the simulations. If this difference in initial thickness would be accounted for, it is probable that the distribution after forming would follow the same trend.

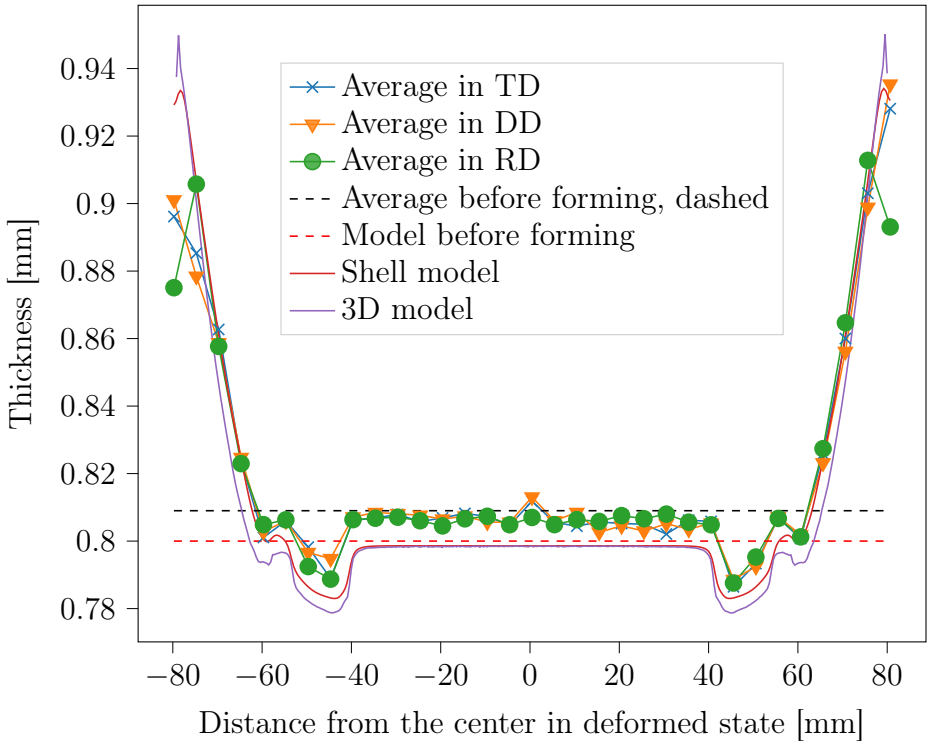

Fig. 19: Average measured cup thickness depending on direction

The primary focus, however, was on the earing profile of the cup, as this phenomenon reflects the material's anisotropy. The experimentally measured cup heights (after tilt compensation) for all four specimens considered, along with their average, are shown in Fig. 20. As previously stated, the earing profile is clearly symmetrical with a 180° periodicity across all specimens. All of the specimen profiles consistently reveal that the material undergoes greater deformation at 135° (–45°) compared to 45°, indicating behavior that cannot be captured by a model assuming quarter-symmetry of the sheet. The abrupt peaks observed at 0° and 180° are remnants from the water jet cutting process, which also aided in identifying the RD after forming.

This phenomenon is quite unusual and could arise from several potential causes. Since the sheets were placed into the testing device with random orientations, a systematic issue with the drawing test itself, such as uneven lubrication, tool wear, or misalignment, is unlikely, especially given the consistent behavior observed across all specimens. However, the sheet normal was not marked, so if some samples were flipped during testing, the asymmetry could be mitigated by averaging the higher and lower cup height values. For this study, all the samples were grouped according to their behavior, emphasizing this effect.

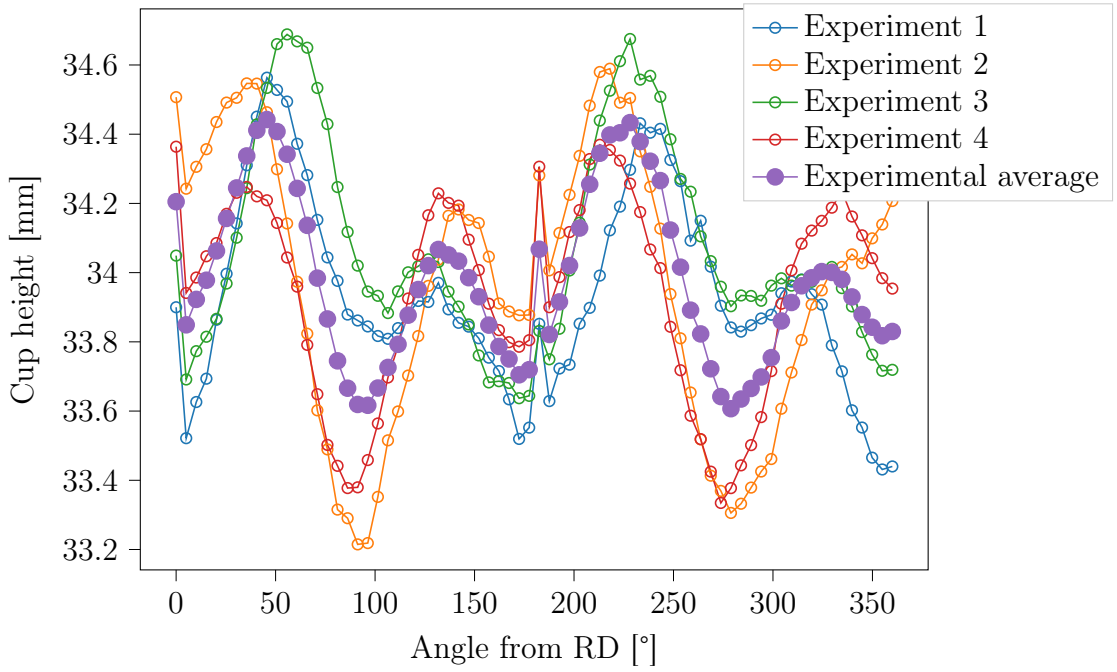

Fig. 20: Measured cup height depending on direction

Another possible explanation is inaccurate calibration of the cutting machine, which may have produced samples that were not perfectly circular—potentially leading to the uneven earing observed. Lastly, the possibility that the asymmetry is an inherent material property introduced during the sheet rolling process, cannot be ruled out. Nevertheless, due to this only partial symmetry, one half of the circular sheet was modeled for use with the Yld2004-18p criterion.

5.1 Comparison of anisotropy

The anisotropy of the material, as already mentioned, was determined by the earing of the cup. Since the all the different YP determination methods and anisotropy models required a separate computation, the impact of each change has to be studied separately. Firstly, the isotropic models were created, differing only in the YP found and the corresponding flow curve. The difference between these models can be seen in Fig. 21. It is clear, that the higher the yield strength is identified, the lower the value of cup height observed. The overall impact of the YP determination method however, is very small.

The height difference between the cup simulated using the flow curve with the lowest yield strength (264 MPa) and the mean value of experimental data is approximately 0.125 mm, while the difference between the highest (587 MPa) and lowest yield strength models is only 0.027 mm. The cup formed with the help of temperature minimum (with the highest yield strength value in TD) is therefore the most accurate, but still overestimates the mean average of cup height by about 0.098 mm.

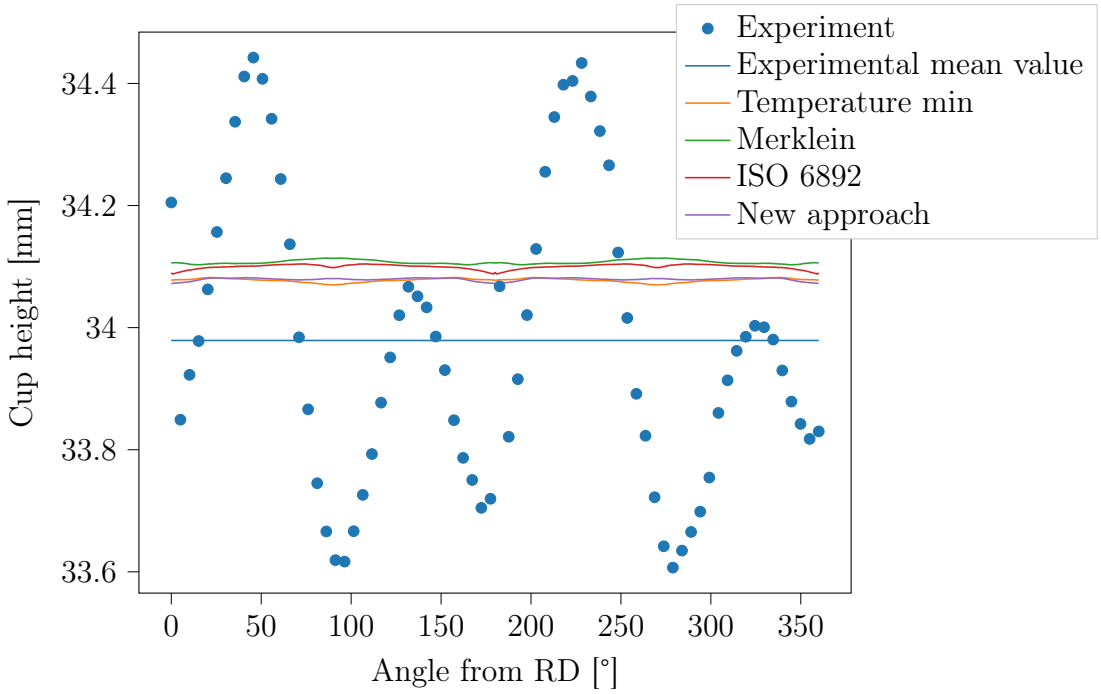

Fig. 21: Isotropic models of different approaches to determining YP in comparison with experimental results

Next, the Hill48r variation of the models is compared based on the YP determined by different methods. As expected, the models do not differ significantly, since all anisotropic coefficients remained nearly identical. The resulting cup height profiles are shown in Fig. 22. It is evident that the anisotropy is overstated, likely due to the experimental spread in r-values, and all profiles are essentially shifted in accordance with the differences in yield strength, similarly to the isotropic case.

The Hill48σ models, on the other hand, generally demonstrate very promising agreement with the experimental data, effectively capturing the overall earing characteristics with the exception of the Merklein [8] YP determination method, which overestimated the earing amplitude to the point of degrading mesh quality and exhibited an out-of-phase response. The remaining methods provided accurate predictions, as illustrated in Fig. 23. Among these, the ISO 6892 approach was identified as the most reliable predictor. The newly developed method showed behavior comparable to the temperature minimum approach, while yielding results that more closely match the experimental observations. It is worth mentioning that since the experimental values used to calibrate this criterion were from 0°, 45° and 90° to RD, the criterion tends to copy the higher peak of experimental curve at 45°. It is possible that if the tensile test used was oriented in -45° to RD that the anisotropy would copy the lower peak values.

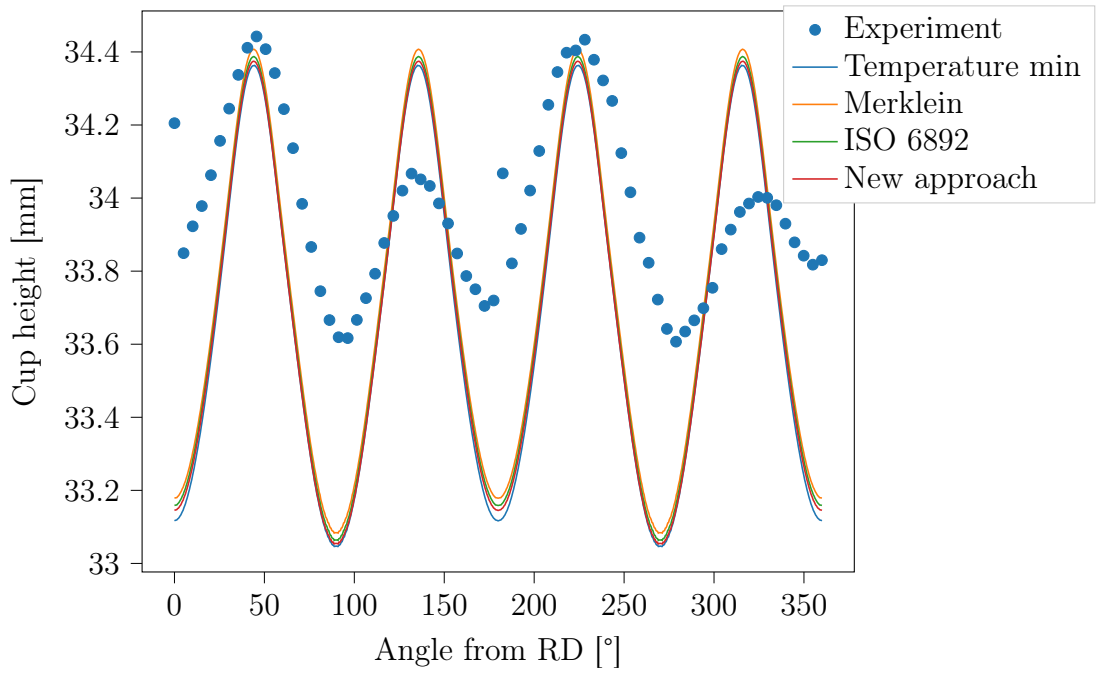

Fig. 22: Hill48r models of different approaches to determining YP in comparison with experimental results

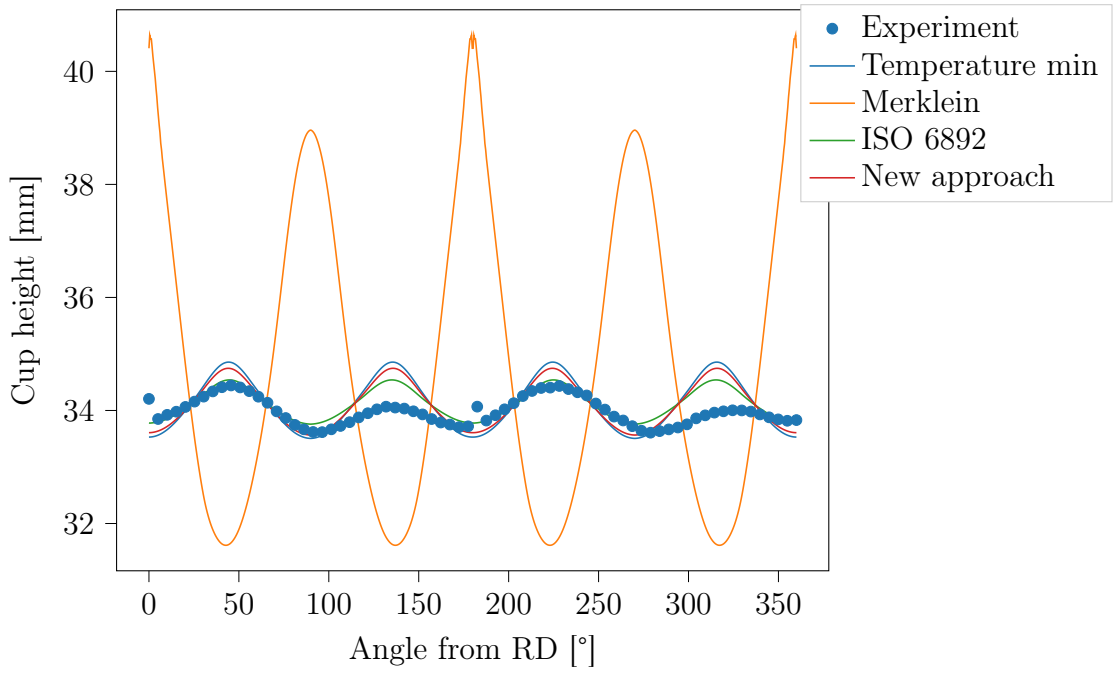

Fig. 23: Hill48σ models of different approaches to determining YP in comparison with experimental results

The Hill48*opt* model, which combines r-values with the identified YP, generally performed slightly worse than the Hill48σ model, as illustrated in Fig. 24. While the Hill48σ model achieved higher accuracy in predicting the earing amplitude, the inclusion of r-values in Hill48*opt* (although with a weight of 0.1) somewhat degraded this precision. The Merklein model [8] continued to exhibit a higher earing amplitude than the other models with mesh being again somewhat degraded, despite the influence of the r-values in Hill48*opt* reducing this amplitude noticeably compared to Hill48σ. Nevertheless, it remains out of phase and fails to predict the correct orientation of the earing peaks.

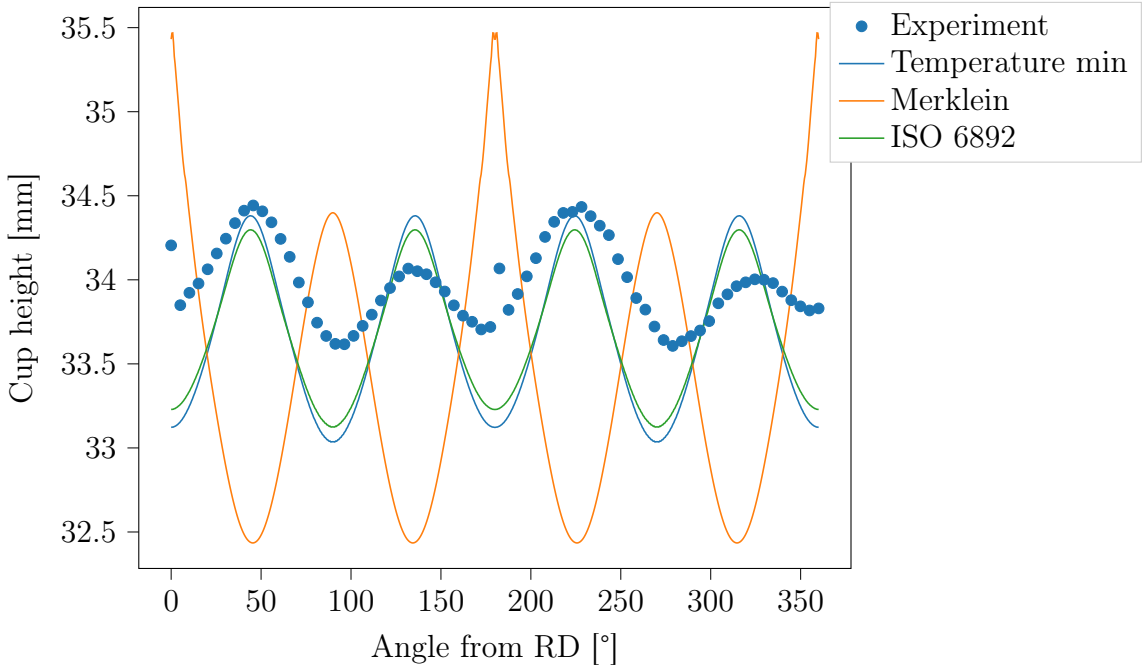

Fig. 24: Hill48*opt* models of different approaches to determining YP in comparison with experimental results

The Yld2004-18p model, when calibrated using all available experimental data, proved challenging to predict due to the absence of direct physical interpretation of its parameters. Significant variations in parameter values often led to only minor changes in the resulting predicted yield strength and r-values. This indicates that the objective function in the 18-parameter optimization is relatively flat and may contain multiple local minima. Consequently, only three models were generated under this criterion, and the corresponding earing profiles are shown in Fig. 25. It is evident that the new YP determination approach was not well-suited for this particular criterion, as it resulted in out-of-phase earing predictions. This discrepancy is likely caused by the unusually low average yield strength at 75°, highlighting how a single outlier can disproportionately affect the overall fit. The amplitude however, matches the behavior very well and the error of this model is therefore paradoxically the lowest. In contrast, the ISO 6892 and temperature minimum criteria delivered more consistent behavior, leading to predictions that aligned more closely with experimental observations. Of the two, the temperature minimum method provided the best agreement, as the experimental data exhibited a smooth anisotropic response, but the amplitude of the cup height is still overestimated.

From each of the anisotropic models the best match is chosen and compared in Fig. 26. It is clear that none of the models was able to capture the asymmetry along the TD. This is of course logical, since both models were calibrated using only 0° to 90° uniaxial tensile tests, making the prediction of different behavior at -45° impossible. If -90° to 90° samples were made, this phenomenon could be potentially studied more in depth and it would be clear if it is material behavior or experimental error. However, from the used models, the overall cup height level seems to be higher for the Hill48σ and Yld2004-18p models and lower for Hill48r and Hill48opt. In all the models present, the anisotropy of the circular sheet is overstated with the mildest anisotropy, using the Hill48σ model, being the most accurate.

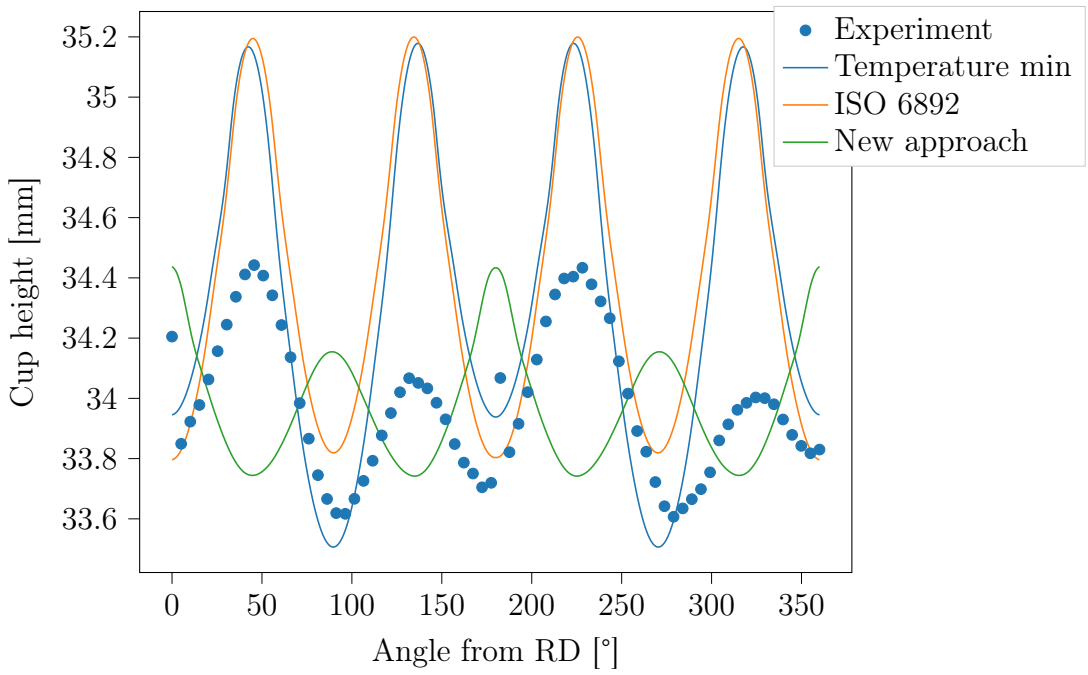

Fig. 25: Yld2004-18p models of different approaches to determining YP in comparison with experimental results

All of the various methods alongside with anisotropic models were then compared according to the mean absolute error (MAE) given by

$$\mathrm{MAE} = \frac{\sum_{i=1}^{n} |y_i - x_i|}{n}, \tag{35}$$

where n is the number of data points and y_i and x_i are the model and experimental data respectively. The errors of the models were calculated for the average experimental cup height and are presented in table 3.

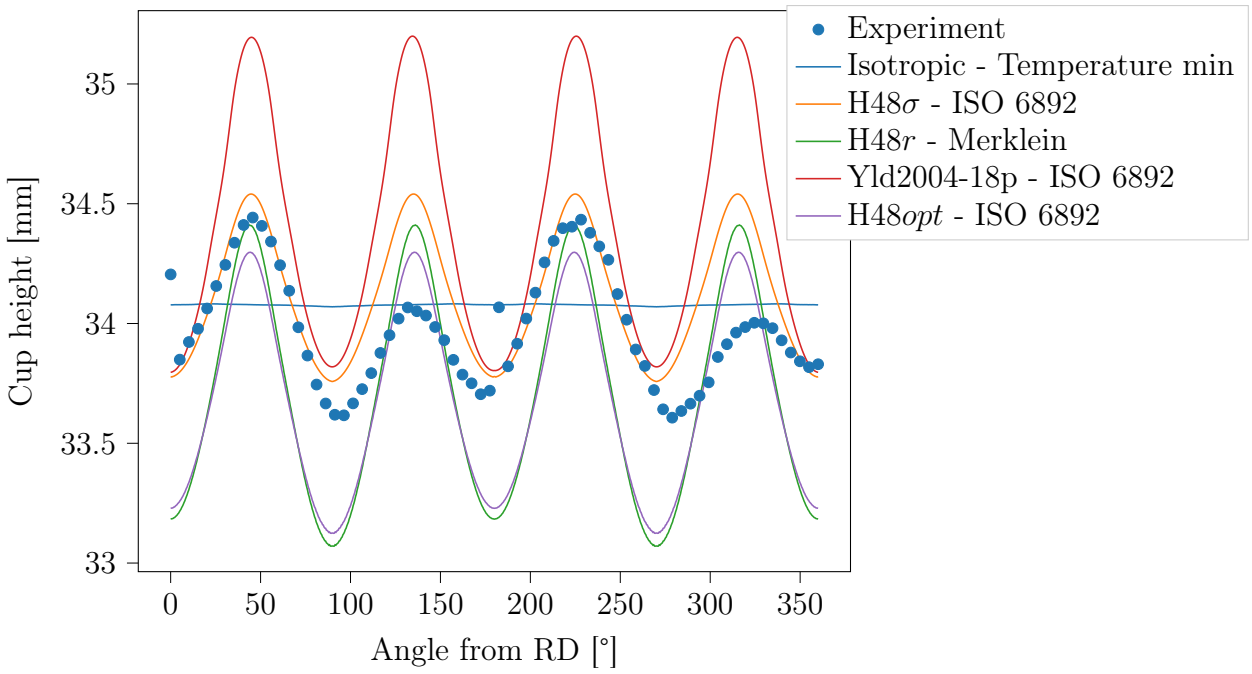

Fig. 26: Different models and their effect

YP determination method	Model variation	Mean absolute error [mm]
ISO 6892-1	Izotropic model	0.231
	Hill48σ	0.173
	Hill48r	0.376
	Hill48opt	0.358
	Yld2004-18p	0.446
Temperature minimum	Izotropic model	0.221
	Hill48σ	0.287
	Hill48r	0.395
	Hill48opt	0.393
	Yld2004-18p	0.418
Merklein	Izotropic model	0.235
	Hill48σ	2.629
	Hill48r	0.366
	Hill48opt	0.954
New approach	Izotropic model	0.222
	Hill48σ	0.239
	Hill48r	0.385
	Hill48opt	0.376
	Yld2004-18p	0.333

Table 3: Values of error in earing prediction according to the different YP determination methods and anisotropic models

From these values is clear, that the most consistent method for YP determination is the ISO 6892-1 because it detects the anisotropy basically at 0.2% plastic strain. This creates more mild anisotropy and robust method for determination since when plastic strain is involved, the stress variation is significantly lowered. Therefore, it is possible that if offset yield strength was considered for the various methods, the anisotropy would behave more in accordance with the experimental results.

The concept of offset yield strength could help isotropic models better align with the actual mean values observed in the results. However, the experimental sheets were thicker than those used in the model by 0.009 mm, and the measurements were prone to significant error due to the generally low cup height. As a result, it is entirely possible that no additional plastic offset would be necessary. Moreover, measuring the cup height proved challenging as changing the reference point from which the height was measured had a substantial (relative) impact on the results.

When it comes to the anisotropic models, the most consistent behavior in this study yielded the Hill48σ model while using an averaged equibiaxial yield strength value averaged from the tensile tests as in [25]. The overall prediction was usually with the closest amplitude and phase except for the Merklein [8] determination method. The Hill48r created mostly the same behavior across all YP determination methods as the anisotropic coefficients did not change substantially with the change of Young's modulus. It also overestimated the anisotropy of the material. The Hill48opt model copied more the behavior of the Hill48r model while having only tenth of the weight coefficient on the predicted r-value compared to the yield strength value. The most complex Yld2004-18p criterion behaved unpredictably as it can be very sensitive to outliers in experimental data used to calibrate the model. The anisotropy was mostly overestimated with the use of this model.

6 Conclusion

In conclusion, it can be stated that all the objectives set in the assignment of this thesis were successfully met. In the introductory part of this work, in addition to an assessment of the current state of the issue, the basic theoretical background was presented. The first part of the analyses carried out in this work focused on uniaxial tensile tests in 7 directions, distributed equally from the rolling direction to the transverse direction, that were performed on the studied material DP1000 to obtain the yield point dependence on the angle of the specimen. To determine it, six methods in total were considered, each differing in the approach to the determination of the interval of Young's modulus. Some used the strain-stress curve such as an approach by Merklein [8] and method specified in ISO 6892-1. Others used temperature measurement as the referential signal. This included mostly methods compared in article [19], however these methods were deemed not robust enough for the data quality measured during this research, since they used derivatives of the temperature signal. Therefore, they were not employed in next parts of this thesis. For this reason, a new approach was proposed together with the thesis supervisor and was compared with the temperature minimum as another valid yield point determination method.

In the next part of the thesis, all of the uniaxial tensile tests were used to calibrate two anisotropic models: Hill48 and Yld2004-18. The Hill48 model, using only three directions for calibration (0°, 45° and 90° to the rolling direction), had three variants which all differed substantially. The Hill48σ model which used only yield strength values from the uniaxial tensile tests, describing the anisotropy by stress. The second used model was Hill48r, which used the Lankford coefficients in said directions, describing the anisotropy by deformation. Last calibration variant was Hill48opt, which combined the yield strength values with the Lankford coefficients into an error function to be minimized. The Yld2004-18p model on the other hand was calibrated only using error function but because of the overall complexity of the model and lack of physical meaning of the constants, its behavior was highly unpredictable.

Subsequently, a deep drawing circular cup test was performed, where the main focus was a correct prediction of earing. Since the test was not performed according to EN 1669 standard, it was also necessary to verify the validity of the test. It was found that the eccentricity of the testing device yields inconsistent results and that the dimensions of the setup play a significant role on the forming process. Nevertheless, it was found that it is possible to measure the earing effect even using dimensions outside of the range specified by the standard. The cup height did not differ much in the rolling direction and transverse direction, but at 45° and 135° to the rolling direction, there was a clear difference in the cup height for all the specimens. The cause of this behavior is unclear, but neither experimental error nor material behavior cannot be ruled out.

Lastly, FE model was created to evaluate all of the material models and compare them on the example of the deep drawing cup test. It was first tuned to replicate important aspects of the deep drawing cup test such as the force response and the thickness distribution and then all of the material models and yield point determination methods were compared based on their behavior and overall proximity to average experimental earing results. It was found that the Hill48σ model yields the best results for the majority of methods. The Hill48r and Hill48opt models yield similar results, overestimating

the cup height variation along its circumference and the Yld2004-18p model also mostly overestimates the anisotropy in addition to being significantly more complex. Contrary to current literature, where this model usually performs better than Hill48, it proved to be unsuitable for the very mild anisotropy seen in this study. Overall, as all models were calibrated using tensile tests conducted only between 0° and 90° relative to the rolling direction, none could capture the asymmetrical behavior observed at 45° and 135°.

In summary, achieving more accurate predictions of cup earing during deep drawing with the mildly anisotropic DP1000 material may be better supported by using less complex anisotropic models. This is due to the relatively high variation in yield point predictions across the different methods evaluated. Among these, the ISO 6892-1 and temperature minimum methods produced the most consistent results. However, even with these methods, the Yld2004-18p model did not outperform the simpler Hill48σ model. Therefore, future research should prioritize minimizing relative differences in yield strength values in different directions rather than focusing on the absolute yield onset when selecting or developing yield point determination method as that seems to have a lower impact on the deep drawing process. Additionally, before adopting a complex anisotropic model, it is advisable to first evaluate the influence of experimental variability on its performance. In addition, further investigation into the influence of offset yield strength on material models could enhance the accuracy of simulation outcomes.

Appendix

For completeness, the following appendix presents the values of yield strength and Lankford coefficients as determined by various methods for yield point evaluation. These values are provided to offer a more detailed comparison of the influence that different yield point determination techniques may have on the mechanical characterization of the material DP1000.

ISO 6892-1	E in TD [MPa]	214085
$r-$values	$\theta = 0°$	0.72104
	$\theta = 15°$	0.87819
	$\theta = 30°$	0.89064
	$\theta = 45°$	0.81826
	$\theta = 60°$	1.02129
	$\theta = 75°$	0.72731
	$\theta = 90°$	0.63629
Yield strength [MPa]	$\theta = 0°$	393.3
	$\theta = 15°$	391.8
	$\theta = 30°$	381.5
	$\theta = 45°$	383.1
	$\theta = 60°$	375.7
	$\theta = 75°$	388.4
	$\theta = 90°$	391.0

Values from uniaxial tensile experiments calculated according to ISO 6892-1

Merklein [8]	E in TD [MPa]	228607
$r-$values	$\theta = 0°$	0.72197
	$\theta = 15°$	0.88015
	$\theta = 30°$	0.89060
	$\theta = 45°$	0.81823
	$\theta = 60°$	1.02154
	$\theta = 75°$	0.72698
	$\theta = 90°$	0.63456
Yield strength [MPa]	$\theta = 0°$	301.6
	$\theta = 15°$	260.9
	$\theta = 30°$	370.1
	$\theta = 45°$	389.1
	$\theta = 60°$	405.5
	$\theta = 75°$	310.9
	$\theta = 90°$	264.1

Values from uniaxial tensile experiments calculated according to the study by Merklein [8]

Temp min	E in TD [MPa]	189988
$r-$values	$\theta = 0°$	0.72325
	$\theta = 15°$	0.88096
	$\theta = 30°$	0.89350
	$\theta = 45°$	0.82183
	$\theta = 60°$	1.02591
	$\theta = 75°$	0.72847
	$\theta = 90°$	0.63983
Yield strength [MPa]	$\theta = 0°$	606.4
	$\theta = 15°$	619.3
	$\theta = 30°$	586.8
	$\theta = 45°$	571.5
	$\theta = 60°$	581.3
	$\theta = 75°$	546.5
	$\theta = 90°$	587.5

Values from uniaxial tensile experiments calculated using temperature minimum

New approach	E in TD [MPa]	189988
$r-$values	$\theta = 0°$	0.72187
	$\theta = 15°$	0.87615
	$\theta = 30°$	0.88946
	$\theta = 45°$	0.82357
	$\theta = 60°$	1.01558
	$\theta = 75°$	0.73203
	$\theta = 90°$	0.63765
Yield strength [MPa]	$\theta = 0°$	504.55
	$\theta = 15°$	485.48
	$\theta = 30°$	479.08
	$\theta = 45°$	479.02
	$\theta = 60°$	464.72
	$\theta = 75°$	374.23
	$\theta = 90°$	489.72

Values from uniaxial tensile experiments calculated using the new approach

References

[1] D. Banabic. *Sheet metal forming processes: constitutive modelling and numerical simulation*. Springer Science & Business Media, 2010.

[2] K. Roll, T. Lemke, and K. Wiegand. Possibilities and strategies for simulations and compensation for springback. In *AIP Conference Proceedings*, volume 778, pages 295–302. American Institute of Physics, 2005.

[3] M. Rossi, A. Lattanzi, L. Morichelli, J.M.P. Martins, S. Thuillier, A. Andrade-Campos, and S. Coppieters. Testing methodologies for the calibration of advanced plasticity models for sheet metals: A review. *Strain*, 58(6):e12426, 2022.

[4] Y. Hou, J. Min, A.A. El-Aty, H. N. Han, and M.-G. Lee. A new anisotropic-asymmetric yield criterion covering wider stress states in sheet metal forming. *International Journal of Plasticity*, 166:103653, 2023.

[5] Li Sun and R.H. Wagoner. Complex unloading behavior: Nature of the deformation and its consistent constitutive representation. *International Journal of Plasticity*, 27(7):1126–1144, 2011.

[6] J. Lee, J.-Y. Lee, F. Barlat, R.H. Wagoner, K. Chung, and M.-G. Lee. Extension of quasi-plastic–elastic approach to incorporate complex plastic flow behavior – application to springback of advanced high-strength steels. *International Journal of Plasticity*, 45:140–159, 2013.

[7] F. Barlat, J.J. Gracio, M.-G. Lee, E. F. Rauch, and G. Vincze. An alternative to kinematic hardening in classical plasticity. *International Journal of Plasticity*, 27(9):1309–1327, 2011.

[8] S. Suttner and M. Merklein. A new approach for the determination of the linear elastic modulus from uniaxial tensile tests of sheet metals. *Journal of Materials Processing Technology*, 241:64–72, 2017.

[9] S. Vitzthum, C. Hartmann, M. Eder, and W. Volk. Temperature-based determination of the onset of yielding using a new clip-on device for tensile tests. *Procedia Manufacturing*, 29:490–497, 2019.

[10] S. Vitzthum, J. Rebelo-Kornmeier, M. Hofmann, M. Gruber, E. Maawad, A.C. Batista, C. Hartmann, and W. Volk. In-situ analysis of the thermoelastic effect and its relation to the onset of yielding of low carbon steel. *Materials and Design*, 219:110753, 2022.

[11] G.I. Taylor and H. Quinney. The latent energy remaining in a metal after cold working. *Proceedings of the Royal Society of London. Series A, Containing Papers of a Mathematical and Physical Character*, 143(849):307–326, 1934.

[12] R. Weichert and K. Schönert. Heat generation at the tip of a moving crack. *Journal of the Mechanics and Physics of Solids*, 26(3):151–161, 1978.

[13] R. Hill. A theory of the yielding and plastic flow of anisotropic metals. *Proceedings of the Royal Society of London. Series A. Mathematical and Physical Sciences*, 193(1033):281–297, 1948.

[14] W.F. Hosford. On yield loci of anisotropic cubic metals. In *Proceedings of the Seventh North American Metal working Conference SME*, pages 191–197, 1979.

[15] F. Barlat and O. Richmond. Prediction of tricomponent plane stress yield surfaces and associated flow and failure behavior of strongly textured f.c.c. polycrystalline sheets. *Materials Science and Engineering*, 95:15–29, 1987.

[16] F. Barlat, D.J. Lege, and John C. Brem. A six-component yield function for anisotropic materials. *International Journal of Plasticity*, 7(7):693–712, 1991.

[17] A. Hybler. Determination of yield surface of material DP1000. Bachelor's thesis. *Pilsen: University of West Bohemia in Pilsen, Faculty of Applied Sciences*, 2022.

[18] W. Thomson. IX.— On the Dynamical Theory of Heat. Part V. Thermo-electric Currents. *Transactions of the Royal Society of Edinburgh*, 21(1):123–171, 1857.

[19] C. Hartmann, S. Vitzthum, L. Maier, and W. Volk. Model-Based Evaluation of Methods for the Determination of the Onset of Yielding by Temperature Measurement. In *International Conference on the Technology of Plasticity*, pages 447–456. Springer, 2023.

[20] A. Lipski. Change of specimen temperature during the monotonic tensile test and correlation between the yield strength and thermoelasto-plastic limit stress on the example of aluminum alloys. *Materials*, 14(1):13, 2020.

[21] R. von Mises. Mechanics of plastic deformation of crystals. *Zeitschrift für Angewandte Mathematik und Mechanik*, 8:161–185, 1928.

[22] Dassault Systèmes. *Abaqus 2023 Documentation.*

[23] R. Hill. *The mathematical theory of plasticity.* Oxford university press, 2003.

[24] H. Quach and Y.-S. Kim. Effect of non-associated flow rule on fracture prediction of metal sheets using a novel anisotropic ductile fracture criterion. *International Journal of Mechanical Sciences*, 195:106224, 2021.

[25] W. Volk, J.K. Kim, J. Suh, and H. Hoffmann. Anisotropic plasticity model coupled with strain dependent plastic strain and stress ratios. *CIRP Annals*, 62(1):283–286, 2013.

[26] A.A. Camberg and T. Tröster. A simplified method for the evaluation of the layer compression test using one 3D digital image correlation system and considering the material anisotropy by the equibiaxial Lankford parameter. In *IOP Conference Series: Materials Science and Engineering*, volume 967, page 012077. IOP Publishing, 2020.

[27] B. Sener. Description of Anomalous Behavior of Aluminum Alloys with Hill48 Yield Criterion by Using Different Experimental Inputs and Weight Coefficients. *Journal of Applied and Computational Mechanics*, 7(3):1606–1619, 2021.

[28] M. Härtel, S. Pfeiffer, S. Schmaltz, B. Söhngen, D. Kulawinski, K. Willner, S. Henkel, H. Biermann, and M.F.-X. Wagner. On the identification of an effective cross section for a cruciform specimen. *Strain*, 54(1):e12257, 2018.

[29] M. Graser, M. Lenzen, and M. Merklein. On the inverse identification of Lankford coefficients using geometrical changes under quasi-biaxial loading. *International Journal of Material Forming*, 12:1053–1061, 2019.

[30] F. Barlat, H. Aretz, J.W. Yoon, M.E. Karabin, J.C. Brem, and R.E. Dick. Linear transfomation-based anisotropic yield functions. *International Journal of Plasticity*, 21(5):1009–1039, 2005.

[31] H. Rong, L. Ying, P. Hu, and W. Hou. Characterization on the thermal anisotropic behaviors of high strength AA7075 alloy with the Yld2004-18p yield function. *Journal of Alloys and Compounds*, 877:159955, 2021.

[32] N. Hosseini and J.A. Rodríguez-Martínez. A simple and computationally efficient stress integration scheme based on numerical approximation of the yield function gradients: Application to advanced yield criteria. *Finite Elements in Analysis and Design*, 192:103538, 2021.

[33] H. Wang, C. Fan, A. Yoshimura, S. Xu, G. Qiu, X. Liang, and J. Yanagimoto. A non-associated constitutive model based on yld2004-18p yield criterion and its applications on sheet metal forming analysis. *Scientific Reports*, 15(1):2797, 2025.

[34] A.M. Habraken, T.A. Aksen, J.L. Alves, et al. Analysis of ESAFORM 2021 cup drawing benchmark of an Al alloy, critical factors for accuracy and efficiency of FE simulations. *International Journal of Material Forming*, 15(5):61, 2022.

[35] J. Coer, H. Laurent, M.C. Oliveira, P.-Y. Manach, and L.F. Menezes. Detailed experimental and numerical analysis of a cylindrical cup deep drawing: pros and cons of using solid-shell elements. *International Journal of Material Forming*, 11:357–373, 2018.

[36] Z. Wang, W. Dong, Q. Lin, and G. Bu. On the earing in cup-drawing with non-uniform die clearance: analytical, numerical and experimental approaches. *Journal of Advanced Mechanical Design, Systems, and Manufacturing*, 15(3):JAMDSM0029–JAMDSM0029, 2021.

[37] K. Bouchaâla, M.F. Ghanameh, M. Faqir, M. Mada, and E. Essadiqi. Numerical investigation of the effect of punch corner radius and die shoulder radius on the flange earrings for AA1050 and AA1100 aluminum alloys in cylindrical deep drawing process. *Heliyon*, 7(4):e06662, 2021.

[38] S. Vitzthum, M. Gruber, J. Rebelo-Kornmeier, M. Hofmann, and W. Volk. Experimental Investigation of Factors Influencing the Determination of the Onset of Yielding by Temperature Measurement. *Key Engineering Materials*, 926:1021–1029, 2022.

[39] D. Banabic and J. Huetink. Determination of the yield locus by means of temperature measurement. *International Journal of Forming Processes*, 01 2006.

[40] D. Banabic and K. Siegert. Anisotropy and formability of AA5182-0 aluminium alloy sheets. *CIRP Annals*, 53(1):219–222, 2004.

[41] M.V. Upadhyay, T. Panzner, S. Van Petegem, and H. Van Swygenhoven. Stresses and strains in cruciform samples deformed in tension. *Experimental mechanics*, 57:905–920, 2017.

[42] N. Deng, T. Kuwabara, and Y.P. Korkolis. Cruciform specimen design and verification for constitutive identification of anisotropic sheets. *Experimental Mechanics*, 55:1005–1022, 2015.

[43] J. Šlegl. Advanced metal sheet testing tool – Bulge test. Bachelor's thesis. *Pilsen: University of West Bohemia in Pilsen, Faculty of Mechanical Engineering*, 2023.

[44] R. J. Espí García (rodrigo.espi.garcia@gmail.com). Anisotropy Calculator.

Linguistic and stylistic revisions to several parts of the text were made based on suggestions generated by ChatGPT.